DEPOSITION AND CHARACTERIZATION OF Ti-Si-N FILMS BY SPUTTERING

A DISSERTATION

Submitted in partial fulfillment of the requirements for the award of the degree

of

MASTER OF TECHNOLOGY

in

METALLURGICAL & MATERIALS ENGINEERING

(With Specialization in Corrosion Engineering)

By

SATPAL JAIN

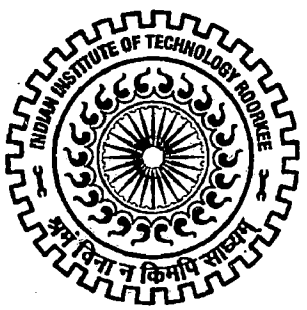

DEPARTMENT OF METALLURGICAL & MATERIALS ENGINEERING
INDIAN INSTITUTE OF TECHNOLOGY ROORKEE
ROORKEE -247 667 (INDIA)
JUNE, 2006

CANDIDATE'S DECLARATION

I hereby declare that the work, which is being presented in the Dissertation entitled **"DEPOSITION AND CHARACTERIZATION OF Ti-Si-N FILMS BY SPUTTERING"** in partial fulfillment of the requirement for the award of the degree **MASTER OF TECHNOLOGY** in **Metallurgical and Materials Science Engineering** with Specialization in **Corrosion Engineering,** and submitted in the **Department of Metallurgical and Materials Engineering** of **Indian Institute of Technology Roorkee**, under the kind guidance of **Dr.R.JAYAGANTHAN**, Department of Metallurgical and Materials science Engineering & **Dr. RAMESH CHANDRA** ,Institute Instrumentation Centre, Indian Institute of Technology, Roorkee, has not been submitted by me for the award of any other degree of this or any other Institute / University.

Place: Roorkee
Date: 28/6/06

Satpal Jain
(SATPAL JAIN)

This is to certify that the above statement made by the candidate is correct to the best of my knowledge.

R. Jay

(Dr.R.JAYAGANTHAN)
Assistant Professor
Department of Metallurgical and
Materials Engineering,
Indian Institute of Technology, Roorkee,
Roorkee - 247667

RChandra 26/6/2006

(Dr. RAMESH CHANDRA)
Assistant Professor
Institute Instrumentation Centre
Indian Institute of Technology, Roorkee,
Roorkee-247667

ACKNOWLEDGEMENT

The Lord has given me strength to persevere in difficult times and brought the people mentioned below to help me through this journey.

I express my sincere gratitude towards Dr.R.JAYAGANTHAN, Department of Metallurgical and Materials Engineering & Dr. RAMESH CHANDRA, Institute Instrumentation Centre, Indian Institute of Technology, Roorkee (India), for their guidance, advice, support and encouragement during the whole span of Dissertation. Without them, the completion of this work would not have possible.

I express my deep sense of gratitude towards Dr. P.S.MISHRA, Head of the department of Metallurgical and Materials Engineering, IIT Roorkee, for his inspiration and co-operation at every stage of this work. I also give sincere thanks to all faculties for their support while completing this work.

I would also like to thank Mr. Amit Kumar Chawla (Research Scholar) for his help rendered during my experiment work.

I would like to thank my family and friends for giving me moral and emotional support.

Date: (SATPAL JAIN)

ABSTRACT

Magnetron sputtering combined with pulsed dc power supply is a powerful tool for the deposition of compound thin films This thesis involves the deposition of superhard nanocomposite coatings of TiN/Si_3N_4 using magnetron sputtering system. The coatings were deposited on silicon substrates using separate Ti and Si target in Ar/N_2 gas mixture under high vacuum conditions. Co-sputtering of single element targets allows an easy adjustment of stoichiometry of deposited films, and ion assisted provides good control of energetic ion bombardment during film growth. An increase in surface mobility provided by this bombardment can enhance the segregation of nanocrystalline TiN in the a-SiN_x matrix, leading to improved mechanical properties.

The effects of the silicon addition, negative substrate bias on the texture development of the films were studied systematically by varying the bias voltage in range -20 V to -200V. The accompanying changes in the microstructure and growth morphology of the phases in these films were investigated in detail using X-ray diffraction, Atomic force microscopy and Nano-indentation technique. Pure TiN films deposited without silicon exhibits strong (111) preferred orientation, while with addition to Si, the orientation of the films changes from (111) to (200). Meanwhile the surface morphology of these films changed from a pronounced columnar microstructure to dense and fine grain structure. The effect of negative substrate bias voltage applied during deposition also resulted in similar change of orientation and leads to increase in hardness of films from 21 to 40 Gpa.

TABLE OF CONTENTS

LIST OF FIGURES

LIST OF TABLES

1 INTRODUCTION

A rapid development in recent years has been seen in the field of nanotechnology due to the existing potential applications of nanomaterials in a wide variety of technological areas such as electronics, catalysis, ceramics, magnetic data storage and structural components. With reduction in size, the materials exhibit peculiar and interesting mechanical and physical properties, e.g. Increased mechanical strength, enhanced diffusivity, higher specific heat and electrical resistivity, compared to the conventional coarse grained counterparts. Nanomaterials include sintered materials with an ultrafine grain structure, loosely segregated nanoparticles and nanocrystalline thin films. In addition to the electronic applications, these materials have tremendous use in the field of tribology because of their enhanced mechanical properties for industrial applications.

Nanostructured and nanocomposite films represent a new generation of materials. Nanocomposite films are composed of at least two separate phases with nanocrystalline and/or amorphous structure. The nanostructured and nanocomposite materials due to (i) very small (10 nm) grains from which they are composed and (ii) a significant role of boundary regions surrounding individual grains behave in a different manner compared to that of conventional materials with grains greater than 100 nm and so exhibit completely new properties.

This new generation of materials exhibits new physical and service properties due to the interaction between grains has significantly changed. The hardness of nanocomposite materials arises from the presence of nanometer scale grains, which hinders the generation and movement of dislocations, stops crack propagation due to the presence of large number of grain boundaries, and suppresses grain boundary sliding .

Nanomaterials can be classified into nanocrystalline materials and nanoparticles. The former are polycrystalline bulk materials with grain sizes in the nanometer range (less than 100 nm), while the latter refers to ultrafine dispersive particles with diameters below 100 nm. Nanoparticles are generally considered as the building blocks of bulk nanocrystalline materials. Research in nanomaterials is a multidisciplinary effort that involves interaction between researchers in the field of physics, chemistry, mechanics and materials science, or even biology and medicine. It has been stimulated by the interest for basic scientific investigations and their technological applications. Nanomaterials and most of the applications derived from them are still in an early stage of technical development. There are several issues that remain to be addressed before nanomaterials will become potentially useful for industrial sectors. These issues include synthesis of high purity materials with large yield economically and environmentally, characterization of new structures and properties of nanophase materials, fabrication of dense products from nanoparticles with full density and less contamination, and retention of the ultrafine grain size in service in order to preserve the mechanical properties associated with the nanometer scale[1].

Novel fabrication technology of nanoparticles is versatile and includes a wide range of vapor, liquid and solid state processing routes. Available techniques for the synthesis of nanoparticles via vapor routes range from physical vapor deposition and chemical vapor deposition to aerosol spraying. The liquid route involves sol-gel and wet chemical methods. The solid state route preparation takes place via mechanical milling and mechanochemical synthesis. Each method has its own advantages and shortcomings [2].

Nanoparticles synthesized from several routes may have different internal structures that would affect the properties of materials consolidated from them. Processing nanoparticles into fully dense, bulk products or coatings which retain the nanometer scale grain size is rather difficult to achieve in practice. Due to their high specific surface areas, nanoparticles exhibit a high reactivity and strong tendency towards agglomeration. Moreover, rapid grain growth is likely to occur during processing at high temperatures. Electrodeposited samples are believed to be free from porosity, but they

contain certain impurities and texture that may degrade their mechanical performances. Therefore, controlling these properties during synthesis and subsequent consolidation procedures are the largest challenges facing researchers.

The unique properties of nanocrystalline materials are derived from their large number of grain boundaries compared to coarse-grained polycrystalline counterpartes. In nanocrystalline solids, a large fraction of atoms (up to 49%) are boundary atoms. Thus the interface structure plays an important role in determining the physical and mechanical properties of nanocrystalline materials .Huang et al. [3] reported that nanocrystalline copper has a much higher resistivity and a larger temperature dependence of the resistivity than bulk copper. They attributed this effect to the grain-boundary enhanced scattering of electrons. Nanocrystalline metals have been found to exhibit creep and superplasticity with high strain rates at lower temperatures than their micro-grained counterparts.

In the past decade, favorable applications have been found for hard and wear-resistant ceramic coatings in industrial sectors. Transition metal nitride coatings are of particular interest due to their high hardness, thermal stability, attractive appearance and chemical inertness. Different techniques are now available for the preparation of Conventional nitride coatings. Thin film, vacuum-based deposition techniques fall into two basic categories: physical vapour deposition (PVD) and chemical vapour deposition (CVD) [4]. PVD techniques include physical sputtering, thermal evaporation and arc-based deposition. Nanocrystalline coatings of transition metal nitrides can be deposited on substrate materials by means of ion beam assisted deposition. The process is based on simultaneous ion bombardment of the growing physical vapor deposited film. This technique is generally atomic in nature, in that the films are deposited from single atoms or small clusters and any reactions that occur, takes place at the film surface independently of the source process. This technique permits the deposition of nanocrystalline nitride films at lower temperatures with better coating-substrate adhesion. This differs from CVD techniques, in which molecular species in the gas phase chemically react at a film surface, resulting in the formation of a condensed

film as well as the emission of volatile by-products. Nanocomposite coatings can be divided into three groups according to their hardness:

(1) The hard coatings with hardness H < 40 GPa;

(2) The superhard coatings with 40≤ H≤ 80 GPa;

(3) The ultrahard coating with H > 80 GPa.

In recent years, there has been increasing interest in the deposition of composite films to answer the scientific and technological requirements in searching for new coating materials. The improvement of tool materials coated with transition metal nitrides has led to interest in developing superhard coatings for wear protection under complex loads and aggressive environments. Optimal microstructural design and materials selection permit chemical, physical and mechanical characteristics can be tailored for specific applications. Superhard coatings having hardness values above 40 GPa are obtainable in multilayer structures with the period of the superlattice (bilayer thickness) within the nanometer regime. The enhancement of superhardness is attributed to a difference in shear modulus between two layer materials and to the presence of sharp interfaces between the layers.

One of the most well known examples is the deposition of TiN-based composites, which have found widespread applications for tools and other hard surfaces . TiN has achieved interesting applications in tribology as a hard coating material applied to cutting tools in terms of enhancing life and performance. However, despite its undoubted success in a wide range of applications, TiN starts to oxidize severely at temperatures as low as 500 ^{0}C. In accordance with the foregoing analysis, it has been found that the oxidation of TiN is considerably decreased by the presence of some less noble elements such as aluminum and chromium. There is a range of similar mixed nitride materials of the general form ((nanocrystalline)-XN)/((amorphous)-YN), where X and Y can be metals and N is nitrogen. These materials have unique properties of superhardness and improved ductility. It is believed that the unique properties of these materials result from the peculiarity of the material structure when nanocrystallites of XN are enveloped by an amorphous phase of YN. One of the

most recent materials is that where small TiN grains are embedded in an amorphous Si $_3N_4$ matrix, the nc-TiN/a-Si $_3N_4$ system [5].

In terms of MD computer simulations, grain-boundary accommodation mechanisms such as grain-boundary sliding and diffusion are considered to be the main factors causing the softening of nanocrystalline materials with grain sizes below 10 nm .Blocking of grain-boundary sliding of nanocrystalline grains embedded in a thin amorphous matrix is believed to be responsible for superhardness of the nanocomposite coatings.

These coatings have been synthesized by DC magnetron sputtering. In general this technique was cleaner and safer, and a lower substrate temperature offers wider choice of substrates and reduced thermal stress.

In this report we use the magnetron sputter deposition (MSD) to prepare nc-TiN/a-SiNx films and the correlation between film properties and preparation conditions. Co-sputtering of single element targets allows an easy adjustment of the stoichiometry of the deposited films, and ion assisted deposition provides good control of energetic ion bombardment during film growth, in terms of both flux and energy. An increase in surface mobility provided by this bombardment can enhance the segregation of nanocrystalline TiN in the amorphous silicon nitride matrix, leading to improve mechanical properties. X-ray diffraction was used to investigate the structure and grain size, and its correlation with hardness behavior as a function of Si content and bias voltage. The preferential growth, as a function of Si content and bias voltage, changes from (111) to a preferred (200) orientation when negative bias voltage and Si content is increased.

Despite the availability of numerous literature data and multidisplinary nature of nanomaterials, a number of problems remain unsolved and the results are not always consistent with each other. To enhance mechanical properties, most films were deposited by adjusting different parameters such as bias voltage and substrate temperature, in addition to silicon concentration.

2 REVIEW OF LITERATURE

2.1 HARD COATING

Hard coatings have been successfully used for protection of materials and particularly to enhance the life of cutting tools since the 1970s. Both the technological process of their production and their properties, i.e. hardness, wear and oxidation resistance, however, are continuously being improved. For development of hard coatings basically these points are always countable (i) to decrease the temperature T at which hard coatings are formed and (ii) to improve the properties of hard coatings, particularly to increase the hardness and oxidation resistance. The oxidation resistance should be increased up to approximately 1000°C because during high-speed machining the temperature of the tool tip can reach 1000°C and the coating should be stable at such high temperatures.

According to hardness their are large number of hard materials but only a few are superhard materials, i.e. cubic boron nitride (c-BN), amorphous diamond-like carbon (DLC), amorphous carbon nitride (a-CN) and polycrystalline diamond. Moreover, these superhard materials are thermodynamically unstable. This is a serious disadvantage which strongly limits their utilization in some applications. For instance, the high chemical affinity of carbon to iron limits the applicability of diamond coated cutting tools to machining of aluminum, their alloys and wood only. Similar problems can be expected when the c-BN coating is used in cutting of steels due to the chemical dissolution of boron in iron. These problems stimulated intensive research in this field, and recently new superhard materials based on superlattices and nanocomposites were developed [6].

2.2 HARD SUPERLATTICE COATINGS

Superlattice coatings are nanometre-scale multilayers composed of two diferent alternating layers with a superlattice period, i.e. the bilayer thickness of two materials, ranging from 5 to 10 nm. The bilayers of these superlattices can be metal layers, nitrides, carbides or oxides of diferent materials or a combination of one layer made of nitride, carbide or oxide of one metal and the second layer made of another metal. According to the composition of the bilayer, superlattice coatings can be divided into five groups: (1) metal superlattices, (2) nitride superlattices, (3) carbide superlattices, (4) oxide superlattices and (5) nitride, carbides or oxides/metal superlattices.

Experiments show that metal superlattices exhibit a relatively low hardness. On the contrary, single-crystal nitride superlattice coatings are superhard materials with a hardness ranging from 45 to 55 GPa [7].

Alloy films with narrow X-ray reflection lines can be converted into films with broad X-ray reflection lines if nitrogen is added, i.e. When the nitride of the alloy film is formed, see e.g. [8]. This means that either binary metal alloys or their nitrides form nanocrystalline films. The structure of the nanocrystalline film can be controlled by the substrate bias, substrate temperature and by the amount of nitrogen incorporated into the film, i.e. by the energy delivered to the growing film.

At present, practically no data are available on oxide superlattice coatings. This is probably because the deposition rate of oxide films using d.c magnetron sputtering is, compared with that of metals, too low. Recently, this situation strongly changed. Considerable progress has been made in magnetron deposition of oxide films, such as Al_2O_3 , ZrO_2 , TiO_2 , etc. using pulsed d.c sputtering . Therefore, oxide films can be produced at economical rates and so we can expect that research will be intensified for oxide superlattice coatings.

It is worthwhile to note that superhard coatings in the form of superlattices represent a very important milestone in the development of superhard materials and the understanding of the origin of the superhardness.

Deposition technique for superhard nanocomposite coating:

Deposition techniques should provide

1) Intense particle bombardment of substrate
2) Sufficient surface mobility
3) High deposition rate
4) Uniform deposition rate
5) Cleaning of Substrate from impurities

Superhard coating can be produced by a number of techniques which can be divided into two broad categories film deposition or surface modification. Available technique for the film deposition include

1) Plasma vapor deposition
2) Chemical vapor deposition

2.3 PHYSICAL VAPOR DEPOSITION

Physical vapor deposition (PVD) is a versatile synthesis method and capable of preparing thin film materials with structural control at the atomic or nanometer scale by careful monitoring the processing conditions. PVD involves the generation of vapor phase species either via evaporation, sputtering, laser ablation or ion beam. In evaporation, atoms are removed from the source by thermal or electron means; in sputtering, atoms are ejected from the target surface by the impact of energetic ions. In the former case, the vapor phase species that experience collisions and ionization are condensed onto a substrate follow by the nucleation and growth. Thermal evaporation has a limitation in multi component materials since one of the metallic elements typically evaporates before the other due to the differences in vapor pressures of the evaporating species. On the contrary, sputtering is capable of depositing high melting point materials such as refractory metals and ceramics, which are difficult to fabricate using evaporation. Since the sputtered atoms carry more energy than the evaporated atoms, the sputter-grown films usually have higher density. Owing to the lower purity of the sputtering target materials,

sputtered films are more prone to contamination than evaporated films.

Inert gas condensation combined with thermal evaporation is commonly used to fabricate metallic and metal-oxide powders with a well defined and narrow size distribution .This technique was originally introduced by Ganqvist and Buhrman [9] in 1976 and developed by Gleiter [10] in 1981. In the process, a metal is evaporated inside an ultrahigh vacuum (UHV) chamber filled with inert gas, typically Argon. Vapors from the hot sources migrate into a cooler gas by a combination of convective flows and diffusion. The vaporized species then lose energy via collisions with Argon molecules. As collisions limit the mean free path, super saturation can be achieved above the vapor source. At high super saturation, the vapors rapidly nucleate, forming large numbers of clusters that grow via coalescence and agglomeration. The size, morphology and yield rate of the clusters in gas-condensation is dependent on three fundamental rates. They are: (1) the rate of supply of atoms to the region of supersaturation where condensation occurs, (2) the rate of energy removed from the hot atoms via the condensing gas medium, and (3) the rate of removal of clusters once nucleated from the supersaturated region

Inert gas condensation using a DC magnetron sputtering source has been used to prepare refractory metal and ceramic nanoparticles. The method of sputtering and gas condensation is crucially dependent on several processing parameters such as gas pressure, sputter power and source- substrate distance. Such parameters must be selected carefully to achieve the formation of nanoparticles rather than the formation of a granular film .

Gonzalez et al. [11] used DC sputtering and gas condensation to obtain nanoparticles of Mo, MoNi and MoW. They reported that the particle size is strongly dependent on the argon pressure for all the materials prepared. The average particle size of Mo decreased from 12 nm at 0.4 mbar to 5 nm at 0.8 mbar. The morphology of Mo and MoNi formed at 0.2 mbar is self-arranged and produces well separated

2.4 CHEMICAL VAPOR DEPOSITION

Chemical vapor deposition (CVD) is a process where one or more gaseous adsorption species react or decompose on a hot surface to form stable solid products. The main steps that occur in the CVD process can be summarized as:

(a) Transport of reacting gaseous species to the surface.
(b) Adsorption of the species on the surface.
(c) Heterogeneous surface reaction catalyzed by the surface.
(d) Surface diffusion of the species to growth sites.
(e) Nucleation and growth of the film.
(f) Desorption of gaseous reaction products and transport of reaction products away from the surface [12].

CVD is a more complex method of forming thin films and coatings than PVD. CVD exhibits several distinct advantages such as the capability of producing highly pure and dense films or fine particles at reasonably high deposition rates, and the capability of coating complex-shaped components uniformly due to its non-line-of-sight nature. CVD is widely used for the deposition of metallic, ceramic and semiconducting thin films. Depending on the activation sources for the chemical reactions, the deposition process can be categorized into thermally activated, laser-assisted and plasma-assisted CVD.

Table 2.1 Comparison of techniques

Chemical vapor deposition	Physical vapor deposition
Intense gas discharge	Low temperature technology
High chemical activity of reactive gas	Many parameter affect grain size
High surface mobility	Less hazardous
Complicated geometry of substrate	Easy to scale up
High thermal stability of nanostructure	Well controlled parameter

But none of them is absolutely perfect because following reasons

Chemical vapor deposition	Physical vapor deposition
High corrosive gases used	Low ion bombardment
High temperature required	Low chemical activity
Problem with scale up	High compressive stress

2.5 REACTIVE MAGNETRON SPUTTERING DEPOSITION

Magnetron sputtering is a thin film deposition technique based on the physical sputtering effects caused by the bombardment of a target material with accelerated ions produced within glow discharge plasma. A wide variety of thin film materials, from metals to insulators, may be produced using this technique. Usually the thin film composition will be determined exclusively by the elements composing the target, since the only elements occurring in the gas phase are the noble gas ions used to generate the plasma and other particles ejected from the target as the result of the sputtering process. In some cases a reactive element may be introduced in the gas phase that will interact with the deposited elements; this latter case is called reactive sputtering. In order to understand the thin film growth processes and the dependence of its characteristics on the system parameters, it is necessary to know how the particles are removed from the target and how they interact on the substrate surface.

2.6 PRINCIPLE OF SPUTTER DEPOSITION

The ejection of atoms from the surface of material (the target) by bombardment with energetic particles is called 'sputtering'. If the sputtering is due to positive ions bombardment, it is referred to as Cathodic sputtering. The ejected or sputtered atoms can be condensed on a substrate to form a thin film. Other processes associated bombardment of a target by highly energetic ions include: (i) secondary electrons reflection at the target surface, (iii) ion implantation, with the ion permanently buried the target, (iv) radiation damage in the structural rearrangement varying from vacancies and interstitial to more gross lattice defects and (v) emission of X-rays and photons . These can be summarized as illustrated in fig.2.1

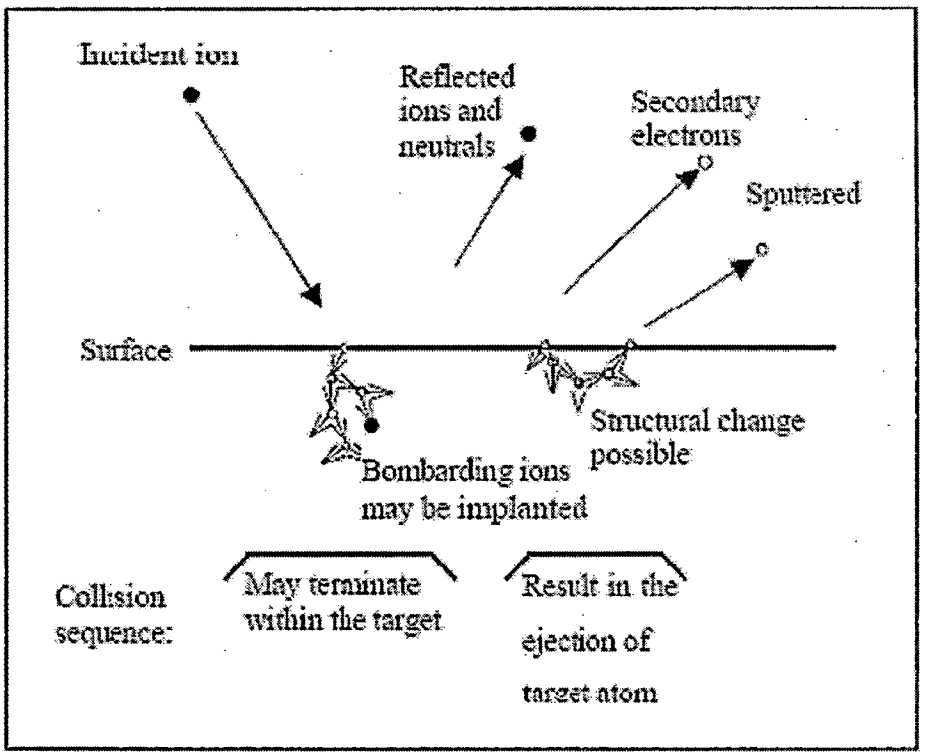

Fig 2.1 Processes generated by the impact of highly energetic particle on a target Si [13]

To obtain sputtering as a useful coating process some criteria have to be met. First of sufficient energy must be created and directed towards the surface of a target to atoms of the surface of the material. To achieve this, a low pressure argon gas for example, can be present in a chamber and by application of a sufficiently large voltage between the target and the substrate, as discussed below; a glow discharge is set up in a way to accelerate the positive ions to the target to cause sputtering. The average ion energy is given by

$$\overline{E} = \frac{2\lambda_p}{L} \cdot eV_c \qquad \text{----------2.1}$$

where L is the separation between the cathode and the anode. λ_p is the mean free path of the sputtering ion. Vc is the cathode fall voltage and e is electron charge. Secondly, the ejected materials must be able to get to the substrate with little impedance to movement. The pressure p determines the mean free path. λ_p,of the sputtered particle. According to paschen relation ion energy is proportional to 1/p .In addition to pressure, the target substrate distance determines the scattering of the sputtered particles on there

way to the substrate and hence also the amount of energy that they deposit on the substrate.

Sputtering is characterized by the sputter yield S, which is the ratio of the ejected atoms to the number of incoming energetic particles, which are predominantly ions. For low bombardment energies, E. up to about 1 keV, equation by Sigmund [13] is used to predict the sputter yield:

$$S = \frac{3\alpha}{4\pi^2} \frac{m_i m_t}{(m_i + m_t)^2} \frac{E}{U_o} \quad \text{----------2.2}$$

Where U_o is the surface binding energy of the material being sputtered, and monotonic increasing function of m_t/m_i for m_i and m_t the ion and target atom masses respectively , with values in the interval of 0.17 and for m_t/m_i between 0.1 and 10.

Reactive sputtering, the method used in this work, involves addition of a gas in the sputtering process thereby producing a material by reaction of the gas sputtered target material. The reaction may be controlled to just dope the film with the desired percentage of the gas or enough gas may be supplied to ensure complete reaction of the sputtered metal.

Disadvantages encountered in reactive sputtering include low film grow and arcing. The latter is caused by a breakdown due to high electric field strength in the thin insulating layer formed adjacent to the target erosion area during reactive sputtering. Low growth rates result from decreased sputter yield for the compounds due to binding energies as is apparent from equation 2.2.

2.7 PLASMA PROCESSES

Glow discharge processes generate ions used in planar magnetron sputtering systems. A glow discharge may be established when a potential is applied between two electrodes in a gas. Once established two or three different regions of plasma can be clearly distinguished between the electrodes. Close to the cathode there is a dark region that exists also near the anode although the latter is generally too thin to be observed. Next there is negative glow region and if the separation between the electrodes is higher than a few times the dark space thickness, a positive column develops between the negative glow and the anode. The positive column is the region that more closely resembles plasma. The plasma does not take a potential between those of the electrodes, but rather acquires a potential slightly higher than that of the anode. Inside the plasma, as expected, the electric field is very low. The main potential difference is therefore observed at the sheaths next to each of the electrodes. The role of the magnetron is forming electron traps that help to sustain the discharge.

Without the magnetron, the electrons emitted from the cathode by ion bombardment are accelerated nearly to the full applied potential in the cathode dark space and enter the negative glow, where they collide with the gas atoms producing the ions required to sustain the discharge. As the electron mean free path increases with gas pressure decrease, at low pressures the ions will be produced far from the cathode where the chances of being captured by the walls are high. At the same time many primary electrons (the ones emitted from the cathode) reach the anode with high energy, inducing secondary electron emission. Therefore, ionization efficiencies are low and self sustained discharges cannot be maintained in planar diodes at pressures below 1.3 Pa . Currents are also limited since voltage increases the primary electron energy and consequently their mean free path. At high pressures the sputtered atom transport is reduced by scattering, which at some point starts to force a decrease in the deposition rate.

On the other hand, with the magnetron system configuration, the primary electron motion is restricted to the vicinity of the cathode and thereby ionization efficiency is increased. This effect is easily obtained imposing a magnetic field parallel to the cathode surface and thus normal to the electric field. In a planar configuration, though, the E x B motion causes the discharge to be swept to one side. This difficulty can be overcome using cylindrical cathodes, which allow E x B to close on themselves [14]. Planar magnetrons can be achieved by

placing the magnets, directly behind the cathode, in a configuration such that at least one region in front of the cathode surface has a closed path which is perpendicular to the magnetic field lines that are parallel to the surface. Although there are many variations in geometry, all have in common a closed path or region in front of a mostly flat cathode surface, where the magnetic field is normal to the electric field. Bounding this region the magnetic field lines enter the cathode surface. Ideally, at the entry points the field lines are perpendicular to the cathode surface. The ionization region is thus confined to an area adjacent to the cathode surface by one or more endless toroidal electron trapping regions, bounded by a tunnel shaped magnetic field.

2.8 THIN FILM GROWTH

In sputtering deposition as in other standard vacuum deposition processes, the material arrives at the substrate mostly in an atomic or molecular form. Using the kinetic theory of gases it is possible to estimate the frequency with which gas particles impinge on a surface, ν, when the gas phase pressure is P:

$$\nu = \frac{P}{\sqrt{2\pi mkT}} \qquad \text{---------- 2.3}$$

In Eq.2.3, m is the mass of the gas particles, k the Boltzmann constant and T the temperature. Considering that for air the mean particle mass is 4.8 x 10~23 g, collision frequency will be approximately 3 x 1024 $cm^{-2}s^{-1}$ at 25° C and 1 atm. Given that a perfectly smooth surface of 1 cm3 has about 1015 atoms, when immersed in a gas at 1 atm pressure, each atom on the surface will be hit about 109 times each second. At 5 x 10^{-3} mbar, collision frequency will be reduced to 1.5 x 10^{19} cm^{-2} s^{-1} which is still a very high frequency. In the case of sputtering the particles that will interest to the film growth will be the ones evaporated from the target and these will have a much lower collision frequency.

The condensed particles may diffuse around the surface, with a motion determined by their binding energy to the substrate, may be incorporated into the lattice or evaporate. Given the high collision frequency of the gas particles inside the deposition chamber these will have a non-negligible influence on the adsorbed particles diffusion. The diffusion process may lead to adsorption, particularly at special site edges or other defects, or the diffusing particle may

desorb. During these processes, characteristic activation energies have to be overcome. The corresponding activation energies for adsorption or diffusion depend on the atomic details of each process and will not be considered now. Besides adsorption and surface diffusion, nucleation of more than one adsorbed particle might occur. Inter diffusion of adsorbed particles with the substrate often happen leading to film-substrate interface smoothing. In thermodynamic equilibrium all processes take place in two opposite directions at equal rates. Therefore, in equilibrium no net film growth would be observed, so that layer growth must be a non-equilibrium kinetic process.

Usually, three distinct modes of film growth may be considered: layer by layer growth mode or Frank- Vander Merve mode; island growth mode or Vollmer- Weber mode and layer-plus-island growth mode, that is also called Stransky - Krastanov mode; each named after the investigators associated with their initial description. In layer by layer growth mode the interaction between the substrate and the layer atoms is stronger than between neighbouring atoms. Each new layer starts to grow, only when the last one is completed. If, on the contrary, the interaction between neighbouring atoms is stronger than the overlayer -substrate interaction, the particles will rather form aggregates over the surface that grow in size and eventually coalesce during film growth. This makes up the island growth mode. The layer-plus-island growth mode is an intermediate case where the film starts to grow layer by layer in a first stage and only afterwards begins the formation of island agglomerates.

In island growth mode, each island is usually a single crystal or contains just a few crystals. On a polycrystalline or amorphous substrate, the orientation of each island will be random and the resultant film will be polycrystalline. On single crystal substrates, the islands orientations may be constrained to a given direction by the substrate structure, so that growth and coalescence leads to the formation of a single crystal film. This case is usually known as epitaxy. If surface atoms have high mobility, they have greater opportunity of finding low energy positions consistent with crystal growth. Knowing that mobility is increased by surface temperature, it is expected that higher substrate temperature will promote crystal growth. The same effect can be achieved by reducing the deposition rate, which gives more time to the adsorbed species to find an energetically favorable lattice position. Epitaxial growth was also found to be promoted by electron or ion bombardment and increased energy of deposited atoms.

The environmental conditions around the substrate during magnetron sputtering deposition deserve also to be mentioned, since they will inevitably affect the film structure obtained. Namely, it was ignored in the above description the effect of the energy of the impinging sputtered atoms, as well as the effect of many other particles that may impact on the surface [15].

In first place there might be contaminants arriving at the substrate. These may result from an internal source, such as outgassing from a heating substrate, or by an external source such as the sputtering gas. If the contaminant atoms are chemically active, the contamination will be particularly effective and can only be minimized by reducing the contaminant partial pressure. If the contaminant source is outgassing, the system may have to be evacuated to a higher vacuum or the sources of outgassing heated in order to reduce the outgassing rate and guarantee a sufficiently low partial pressure of the contaminant during deposition. On the other hand, if the contaminant comes with the sputtering gas there is no way to reduce its partial pressure without affecting simultaneously the sputtering gas pressure. Thus it is very important to use high purity sputtering gases.

The sputtering gas atoms might also become part of the deposited film. Although the sputtering gas used is usually an inert gas, given its high partial pressure when compared with that of the sputtered atoms it is not surprising that some of these atoms happen to be trapped in the growing film. Inert gas atoms, are only expected to be physisorbed, so if substrate temperature is increased during deposition, they are less likely to be adsorbed and at the same time more likely to be subsequently desorbed. However, there exists an appreciable difference between the interaction of fast gas particles and that of thermal neutrals with the surface. Energetic neutrals may result from the reflection and neutralization of ions that impinge on the target. These neutrals, arriving at the substrate, have much higher probability to be embedded in the growing film than thermal neutrals. In fact, it has been observed that nickel films deposited by sputtering in an argon atmosphere have higher argon content than nickel films produced in a similar atmosphere, but using evaporation. Positive ions may also impact on the substrate due to the sheath voltage drop near its surface.

Negative ions and electrons can only reach the substrate if they have enough energy to cross the space-charge sheath. Once again it is necessary to distinguish fast from slow particles. Fast negative ions and electrons are produced in the target and accelerated in the target sheath. These fast particles can have a major influence on the structure and properties of the growing

film and also cause substrate heating. Finally there are also photons arriving at the substrate. Photons can be produced by ion or electron bombardment on any surface or result from relaxation of excited atoms in the glow. In the former case the photons may have high energy, at most as high as the energy of the bombarding particle. Such energies may be, in a sputtering system, of the same order of the accelerating potential at the target, which is usually higher than 200 eV. The main effect of photon bombardment of the substrate will be electron emission, which may also affect the film growth processes occurring at the substrate.

2.9 THE THERMODYNAMIC AND KINETIC CONDITIONS NEEDED

Li et al. [16] suggested that the hardness enhancement, which they obtained was due to precipitation hardening by Si_3N_4 particles formed within the TiN crystals . Within their joint collaboration Veprek, Reiprich and Li realized later [17] that this mechanism of hardening is unlikely because the precipitation hardening (as defined in the standard textbooks) is not possible to occur within 3 to 4 nm small nanocrystals of TiN. This led to the development of the generic design concept for the preparation of superhard nanocomposites that is based on a strong, thermodynamically driven (spinodal) decomposition. In the subsequent papers, Veprek et al. have verified that this concept indeed works in a number of different nc-Me_nN/a-Si_3N_4 (Me = Ti, W, V) and fcc nc-$(Al_{1-x}Ti_x)N$/a- Si_3N_4 , nc- TiN/a-BN, nc-TiN/a-BN/a-TiB_2 systems where hardness of ≥ 50 GPa was achieved as well as for the ultrahard, ternary nc-TiN/a- Si_3N_4 /a- & nc-$TiSi_2$ where the hardness reached 80 to 105 GPa.

These researchers report that the maximum hardness in the nanocomposites appears at about the same silicon content. This corresponds to the situation when the surface of the nanocrystals is covered with about one monolayer of Si_3N_4. The same conclusion applies also for the nc-TiN/a- Si_3N_4 /a- & nc-$TiSi_2$ ultrahard nanocomposites where hardness of 80 to ≥ 100 GPa was found and to the superhard nc-TiN/a-BN and nc-TiN/a-BN/a-TiB_2 nanocomposites .

As an explanation for this behavior these researchers suggested a stabilization of the 5 nanostructure by the strong (spinodal) segregation of the stoichiometric nitrides that results in a sharp and strong interface that avoids plastic

deformation due to the lack of dislocation activity within 3-8 nm small nanocrystals and brittle fracture by crack initiation and growth when the amorphous interface is very thin . Furthermore, the difference in the group electronegativity of Si_3N_4 and TiN that leads to a partial electron transfer to Si_3N_4, and possibly also quantum confinement phenomena may further contribute to the observed stabilization of that nanostructure. The high stability of this nanostructure up to ≥ 1100 °C was confirmed by a number of annealing experiments. Recently these researchers showed that the Si_3N_4 interface also stabilizes the metastable , Al-rich solid solution fcc-$(Al_{1-x}Ti_x)N$ against the decomposition and softening up to 1200 °C . (In pure fcc-$(Al_{1-x}Ti_x)N$ with $x \lesssim 0.6$, the decomposition to fcc-TiN + h-AlN followed by softening of the coatings occurs at about 800-900 °C.)

The understanding of the mechanical properties of these materials was significantly advanced by the recent contribution of A. S. Argon who used the Hertzian theory and the Universal Binding Energy Relation (UBER) in order to show the self-consistency of the hardness measurements reported by Veprek et al. [18]. Accordingly, the strength of these nano-composites is approaching the ideal strength of flaw-free materials. The observed decrease of the hardness with the thickness of the Si_3N_4 interface increasing above about one monolayer was originally attributed to the decreasing threshold for the crack initiation and propagation .

Recent molecular dynamic simulation of the mechanism of plastic deformation in covalently bonded glasses by Demkowicz and Argon provided a new insight into this problem.

Accordingly, the plastic deformation in these materials occurs by localized shear transformations within "fertile" volumina of about 3-4 nm in size. These transformations are triggered by a collective movement of 5-6 atoms, which acts as a kind of nucleation event [19]. Obviously, such a "trigger" cannot work within one monolayer thin amorphous layer. This recent progress in the understanding of the high thermal stability and mechanical properties lends a further support to the generic design concept and to the conditions needed for reproducible preparation of the stable, superhard nanocomposites. Therefore we shall, in the following sections, briefly summarize the

thermodynamic and kinetic conditions required for the formation of such stable nanostructure during the film growth.

2.9.1 THERMODYNAMICS

Stoichiometric transition metal nitrides, such as TiN and Si_3N_4 (or BN) are immiscible. It has to be emphasized that the stoichiometric nitrides are stable, at a given temperature, only when the nitrogen pressure is sufficiently high. At a high temperature and low nitrogen pressure the decomposition, such as $Si_3N_4 \rightarrow 3Si(s) + 2N_2(g)$ occurs. The saturation pressure of nitrogen over Si_3N_4 reaches 1 atmosphere already at temperature of 2151 K.

In reference Veprek and Reiprich [20] have shown by means of a simple thermodynamics calculation of the free energy of the reaction

$$xTiSi_y + (2x \cdot y/3)N_2 = xTiN + (x \cdot y/3)\, Si_3N_4 \quad \text{---------2.4}$$

that sufficiently high pressure of nitrogen is needed to provide the thermodynamic driving force in order to shift the equilibrium of that reaction to the stoichiometric, immiscible TiN and Si_3N_4 (i.e. to the right hand side of reaction 2.4). The nitrogen pressure of 1 mbar is sufficient for that purpose even at high temperatures. These authors also emphasized that: *"At a low nitrogen activity most of the systems will form the thermodynamically stable silicide."* This means that at low nitrogen pressure the equilibrium of reaction (2.4) will shift to the left hand side. we also see the dependence of the equilibrium constant for reaction(2.5) on partial pressure of nitrogen for several relevant temperatures, when only $TiSi_2$ is considered. Comparison with the data we found similar trend for TiSi and Ti_5Si_3. Based on general thermodynamic considerations, similar trend is expected for any other mixed $Ti_xSi_yN_z$ phases.

$$6\, TiSi_2 + 11\, N_2 = 6\, TiN + 4\, Si_3N_4 \quad \text{--------2.5}$$

Following conclusions are drawn from this example:

- At a given temperature, a sufficiently high pressure of nitrogen is needed in order to assure the formation of a fully segregated nanostructure consisting of the stoichiometric TiN and Si_3N_4.
- For the typical deposition temperature of 550 °C (823 K), the chemical equilibrium is shifted far to the right hand side of reaction (2), i.e. stoichiometric, immiscible TiN and Si_3N_4 are formed even at a relatively low nitrogen pressure used in plasma PVD deposition techniques.

- Therefore, the frequently observed formation of Ti_xSi_y phases is due to kinetic constrains as also emphasized in the early paper of Veprek and Reiprich . When testing the nanocomposites for their thermal stability, the annealing should be done in nitrogen and not in vacuum because at a sufficiently high temperature the stoichiometric nitrides loose nitrogen, become substoichiometric, and progressively miscible.

There are similar calculations for the "Ti-B-N" system that was studied by a large number of researchers . The reader should notice, that the somewhat smaller values of the equilibrium constant as compared with much larger number of moles of the compounds and N_2 involved in reaction (2.5) (total 27 mole) than in reaction (2.6) (total 5 mole). In fact, at a given temperature and nitrogen pressure, the chemical equilibrium is shifted further to stoichiometric TiN and BN in this system as one can see from the nitrogen pressures where the lines corresponding to T = 1300 and 1500 K are crossing the line Log $K_p = 0$ (i.e. $K_p = 1$).

$$TiB_2 + N_2 = TiN + 2B \quad \text{----------} \quad (2.6)$$

At a temperature of < 1000 K even a relatively low partial pressure of nitrogen of 10^{-3} -10^{-4} mbar (10^{-6} - 10^{-7} at.) is sufficient to shift the chemical equilibrium of reaction (2.5) towards the immiscible, stoichiometric nitrides TiN and Si_3N_4 (and TiN + BN, eq. (2.6)). Therefore, either a too slow dissociative chemisorption of nitrogen on the surface of the growing film or a too slow kinetics of the phase segregation

during the deposition is the limiting factor that avoids reaching the equilibrium, and thus resulting in the formation of $TiSi_2$ or other silicides Ti_xSi_y (and TiB_2), and even the formation of mixed "Ti-Si-N" phases as reported by Tanaka et al. for Ti-Si-N coatings deposited by vacuum arc evaporation [21] and by Vaz et al. for reactive sputtering [22] . For these reason we discuss the role of kinetics during the phase segregation and formation of stable nanocomposites in the next section

2.9.2 KINETICS

As well known, the thermodynamics describes the equilibrium and the kinetics decides if this equilibrium can be achieved under the given conditions. At given nitrogen pressure in the systems discussed here, the chemical equilibrium shifts more to the segregated, stoichiometric, immiscible nitride phases when the temperature is lowered. This however does not mean that lower temperature is favorable for the formation of the stable nanostructure as pointed out by Veprek and Reiprich: *"Of course, at a low deposition temperature kinetic constrains may cause the formation of metastable phases with a smaller free energy of activation, i.e. of homogeneous ternary mixture ..."* [20] .

This means that even if the nitrogen pressure is high enough but the deposition temperature is low, the kinetics may prevent the system to reach the thermodynamic equilibrium because the spinodal phase segregation is thermodynamically driven but its rate is controlled by the kinetics, i.e. by diffusion.

Therefore it was emphasized already in [20] and repeated in many subsequent papers, that one has to use a sufficiently high deposition temperature: *"The substrate temperature of 550 °C is high enough to assure a low chlorine content, a high structural stability of the deposited films under subsequent thermal load and to check is a sufficient segregation occurs..."* . At a too low temperature, the diffusion and surface mobility are too slow and the fully segregated stoichiometric phases with the strong and sharp boundary cannot be formed.

In order to illustrate this point let us estimate the time needed for Si in TiN to diffuse at a distance of about 5 nm that is approximately equal to the crystallite size

found in these nanocomposites. Because of lack of data of the diffusion coefficients in these systems when the surface of the growing film has another (unknown) composition than the final product, we shall take, as a simple illustrative example, the value of diffusion coefficient for grain boundary diffusion of Si in TiN of $D(T) = 2.5 \cdot 10^{-14} \cdot \exp(-0.3eV/kT)$. The time needed for the diffusion to occur at the distance equal to the crystallite size is of the order of $2.5 \cdot 10^{2}$ and $5 \cdot 10^{4}$ seconds at temperature of 823 K (550 °C) and 300 K, respectively. It is clear that the phase segregation can be completed during the deposition at 550 °C but it can never be reached at room temperature.

Therefore it remains an open question as why some workers tried to deposit the superhard "Ti-Si-N" nanocomposites at room temperature. Even at deposition temperature of≤ 300 °C used by many workers (e.g. [8-11,49,50]), 3 the diffusion time for this case is of the order of 10 seconds, i.e. the phase segregation will hardly be completed during the deposition. Such coatings will show self-hardening (increase of the hardness) upon subsequent annealing, provided the impurity content is sufficiently low as discussed in the next section.

In view of these facts, let us now discuss briefly the results of Hu et al. The maximum hardness reported by these authors at room temperature of about 35 GPa decreased to about 28 GPa when the deposition temperature was increased to 400 °C. This shows unambiguously that the fairly high hardness of 35 GPa of the coatings deposited at room temperature was not due to a formation of nanocomposites. Most probably, this hardness enhancement was due to energetic ion bombardment of the growing films during the deposition, and the decrease of the hardness at a higher deposition temperature was due to the relaxation of the ion-induced hardness enhancement. Incomplete information about the deposition conditions, impurity content and thermal stability in the paper of Hu et al. [23] does not allow us to draw any further conclusion.

Finally, let us emphasize, that the rate of the nitride formation depends, beside of the temperature, also on the partial pressure of nitrogen because, in order to form the stoichiometric nitride, the nitrogen from the gas phase (predominantly N_2) has to be dissociatively chemisorbed on the surface of the growing film. The reactive sticking

coefficient for this process depends on the temperature and surface coverage and is typically orders of magnitude smaller than 1. Thus, even if the nitrogen pressure used in a given experiment is sufficient from the thermodynamical point of view (i.e. the chemical equilibrium is shifted towards the stoichiometric, immiscible nitrides), it may still be too low to assure a sufficiently fast kinetics of the dissociative chemisorption. For this reason, the higher the nitrogen pressure used, the better for the sufficient rate of the adsorption to form the stoichiometric nitrides that is needed for the phase segregation into TiN and Si_3N_4.

2.10 IMPURITIES

A sufficient purity is a necessary pre-requisite for the successful preparation of the majority of materials. Nano-sized and nano-structured materials are particularly likely to be sensitive to impurities because of their high dispersion, i.e. high specific surface area. For example, two years ago Veprek et al. reported on the deposition of pure nanocrystalline silicon (nc- Si) free of amorphous tissue by means of chemical transport in hydrogen plasma as well as by saline strongly diluted with hydrogen when a sufficiently high deposition temperature T_{dep} was used [24]. These results were questioned by several groups, who reported that, when silicon films are deposited from saline diluted with hydrogen, they consist of a mixture of nanocrystalline (nc-Si) and amorphous (a-Si) silicon. When the deposition temperature was increased, the crystalline fraction reached a maximum value of only about 0.4 at $T_{dep} \approx 400$ °C, and above T_{dep} of 500 °C only a-Si was formed.

Streret explained this nanocrystalline-to-amorphous transition theoretically by thermodynamic arguments. However, in some paper Veprek et al. have shown that the contradictory results of Matsuda et al. , Tsai et al. and others were due to minor oxygen impurities present in the discharge[25]. When Veprek et al. controllably introduced oxygen impurities of 0.1 to 0.6 at. % into the H_2/SiH_4 glow discharge during the deposition of the Si-films, they were able to precisely reproduce the results of Matsuda et al.. For these reasons, Veprek et al. were also very careful to control impurities in the superhard nanocomposites. In 1997 and 1998, these researchers reported

that impurities degrade the maximum achievable hardness, and they described what kind of precaution is needed in order to avoid the impurity incorporation into the coatings during plasma CVD. For the measurement of the minor impurities concentration they used elastic recoil detection spectroscopy (ERD) that provides a high sensitivity like Rutherford backscattering (RBS) and X- ray photoelectron spectroscopy (XPS) but a superior dynamic range that is not achievable by RBS or XPS. Based on this analytic technique, Veprek et al. reported that the typical concentration of impurities in their coatings deposited by plasma CVD was: *"Oxygen below 0.07 at.%, chlorine below 0.5 at.% and hydrogen below 0.1 at.%. No other impurities were found either by ERD (resulting in an upper limit of 10 ppm) or by EDX."* More recently these researchers conducted a systematic, quantitative study which shows the maximum achievable hardness that can be obtained with the optimum com position, i.e. with silicon content where the hardness reaches a maximum , as a function of oxygen impurity content . These binary, stoichiometric nc-TiN/a- Si_3N_4 coatings deposited by plasma CVD and by reactive magnetron sputtering in three different apparatuses .

Obviously, for nc-TiN/a-Si_3N_4 nanocomposites deposited by plasma CVD oxygen imurities less than about 0.2 at. % and chlorine content less than about 0.5 at. % are required when the hardness should reach ≥ 50 GPa. When the oxygen impurities content is larger than 0.5 at % the hardness of ≥ 40 GPa cannot be achieved, and for oxygen impurity content larger than about 0.6 at. % the hardness remains below 35 GPa. When the oxygen impurity content is larger than about 1 to 1.5 at.%, no hardness enhancement as a function of Si concentration was found.

More recently Meng admitted [26] , that the oxygen impurities were in the range of 2 at.% .This is in agreement with the data of Veprek at al. reported for nc-TiN/a- Si_3N_4coatings having≥ 1 at.% of oxygen . The effect of chlorine and hydrogen impurities is less dramatic as long as they are below about 0.5 at. % .

The data for coatings deposited by magnetron sputtering show a very similar dependence. For the low content of oxygen, the degradation of hardness seems to

be somewhat less pronounced. Nevertheless, oxygen impurity of ≤ 0.2 at % is needed in order to achieve hardness of about ≥ 50 GPa. This is a stringent requirement, which is not easy to meet by sputtering in conventional deposition units.

Let us however emphasize that during the deposition of such coatings by magnetron sputtering with deposition rates of about ≤ 2 μm/hr and background pressure of water and oxygen in the range of ≥ $2 \cdot 10^{-6}$ mbar (as typically found), one expects the oxygen impurity content to be in the range between ≥ 0.6 and several at.% in agreement with some published results .

The hardness of some nc-TiN/a- Si_3N_4 coatings deposited by magnetron sputtering is ≤ 40 GPa, even though the oxygen content is < 0.2 at.%. This is caused by too high ion bombardment (ion current density) during the deposition, which causes the decrease of oxygen impurity content in the coatings, but simultaneously it hinders the formation of optimal nanocomposite structure . This remark emphasizes, that although the high purity of the coatings is a necessary for achieving the high superhardness, it is not any sufficient conditions because the stable, fully segregated nanostructure is needed as well in order to obtain superhard nanocomposites with the high thermal stability. At the end of this section it should be also mentioned that the hardness of nc-TiN/a- BN/a-TiB_2 nanocomposite coatings deposited by plasma CVD does not shown such strong dependence on the oxygen impurity content.

2.11 CONDITIONS NEEDED TO ACHIEVE ULTRA-HARDNESS OF 80 TO≥ 100 GPA

The ultra-hardness was achieved so far only in ternary and quaternary nanocomposites nc-TiN/a- Si_3N_4/a- & nc-$TiSi_2$ when the surface of all nanocrystals was covered with about one monolayer of Si_3N_4 and the oxygen impurity content was ≤ 0.07 at. %. By This hardness of 80 GPa can be achieved in the nc-TiN/a- Si_3N_4 /a-$TiSi_2$ nanocomposites with silicon content of < 10 at. %,where only amorphous $TiSi_2$ is present. At higher Si-content also nc-$TiSi_2$ precipitates and these nanocrystals have to be also

coated with Si_3N_4.

There is a very narrow compositional range for the coexistence of all three phases, i.e. TiN, Si_3N_4 and $TiSi_2$, and it is not an easy task to meet all these requirements simultaneously.

A disadvantage of these ultrahard nanocomposites is the degradation of their hardness on the time scale of several months, whereas the hardness of the binary nc-TiN/a- Si_3N_4 and nc-TiN/a-BN nanocomposites remained stable over a period of several years. The exact reason for the lower stability of the ultrahard nc-TiN/a- Si_3N_4 /a- & nc-$TiSi_2$ nanocomposites is still not known precisely. Most probably, it is associated with the low structural stability of the $TiSi_2$ phase. It is well known that at a relatively low temperature of 550 °C as used for the deposition, the metastable, orthorhombic base-centered $TiSi_2$ C49 phase is formed that transforms to the stable C54 only above 700 °C. Moreover, this transformation is hindered when the size of the $TiSi_2$ precipitates is too small because of the critical nucleation size required for that transformation is evidently too large [27].

2.12 RELIABILITY OF THE HARDNESS MEASUREMENTS ON SUPERHARD COATINGS

The first obvious concern regards the reliability of the hardness measurements by different groups because the easiest explanation of the differences in the maximum achievable hardness could be explained by errors in the work of Li Shizhi's and Veprek's group, as suggested, among others, by Musil et al.. Veprek et al. neutralized the speculative arguments of Musil et al. and in a series of recent papers these authors provided evidence that their measurements of the hardness meet all the requirements regarding their reliability. Here we briefly summarize their early and recent results [28].

The static indentation hardness is the average pressure under the indenter, L/A C (L is the applied load and A C is the contact area between the indenter and the material being measured) that causes the material to develop fully plastic flow. Considering the relation between the stress and strain for a material that displays a typical elastic - plastic

behavior one can see that after the plastic flow stress under the indenter was reached, and the load is than further increased, the materials deforms plastically increasing the contact area so that the ratio L/A C remains constant. Therefore, if correctly measured, the hardness must be invariant of the applied load. Thus, when the automated load-depth sensing indentation technique is used, the values of the hardness must be independent of the maximum applied load. Already in first paper published in 1995, Veprek and Reiprich reported that "... the hardness has been determined as a function of the maximal applied load and the value of the hardness from the part where it was independent of the applied load has been used"[20]. In Ref. [29], an example of such measurements on nc-TiN/a- Si_3N_4 coatings with hardness of 50 GPa. These researchers also emphasized that using too small loads of < 30 mN may yield incorrect data because of a variety of the "indentation size effects" (ISE). The ISE generally means that the value of hardness depends on the maximum applied load. The ISE can have a variety of reasons as discussed, e.g. In the case of the superhard nanocomposites with load-invariant hardness of about 40 GPa measured with maximum applied load of≥ 50 mN, Veprek et al. reported an increase of the apparent hardness obtained from the automated load-depth sensing technique to 80 GPa when the applied load of 5 mN was used. It should be emphasized, that the correction for tip rounding was done carefully so that the hardness of Si and Sapphire was load-invariant down to this lowest load. Furthermore, also the hardness of the coatings of 40 GPa determined from the size of the remaining plastic deformation (after the indentation) by means of calibrated scanning electron microscope (SEM) was load-invariant within the whole range of applied load between 5 and 100 mN .

In more recent papers, these researchers extended their studies to a variety of superhard nanocomposite coatings in order to verify the self-consistency of the data in terms of Hertzian analysis of the indentation curves [18][21] and also to compare the values of the load-invariant hardness obtained by the load-depth indentation technique with the classical value of hardness $H = 0.927 \cdot L/A_P$ where L is the applied load and A_P the projected area of the indentation that was determined by means of calibrated scanning electron microscope.

Because, for these coatings, the load-invariant values of hardness are found only at a relatively large applied load of 30 to 150 mN, more than 6 μm thick coatings

are needed in order to assure that the indentation depth is larger than about 0.3 μm (to avoid an apparent and incorrect increase of the measured hardness at small load due to ISE but still smaller than about 5 to 7 % of the thickness of the coatings .

To best of our knowledge, no other researchers did this kind of careful measurements on thick coatings using large loads and verifying if the values, which they report, are indeed load-invariant. In majority of the papers, the reported values of hardness were obtained on≤1-2 μm thin coatings and in some papers even less than 0.5 μm thin films and small loads of < 0.1 mN were used. With reference to hardness reported by Meng et al. and by Dieserens et al. for TiN (i.e. for Si- content zero) was about 31 and 28 GPa, respectively. These values are obviously too high because the intrinsic hardness of TiN is about 20-22 GPa. In conclusion to this section it should be clear that Li et al. and Veprek at all did probably the most careful measurements and the criticism addressed to others.

2.13 MATERIALS

Titanium nitride

This transition metal nitride is one of the most diverse coatings, and its applications are found within a variety of technological areas, for example as wear resistant and hard coating on cutting tools and drills, as coating within the medical and health area due to its non-toxic nature, and as diffusion barrier in microelectronics. Titanium nitride (TiN) has also found a market as a decorative coating due to its golden color. Its usefulness is explained by the material properties. It has a rocksalt structure (FCC bravais lattice) with a unit cell consisting of four formula units, shown in Fig. 2. The lattice parameter is equal to 4.240 Å. On top of its high hardness of roughly 18 GPa it has a high melting temperature of 3290 ^{0}C, and density is 5.43 g/cm^{3}.

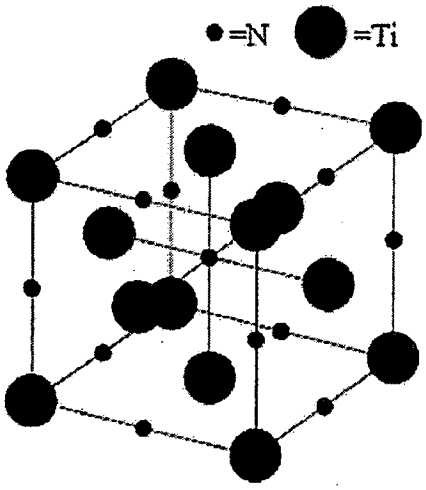

Figure 2.2 Illustration of a TiN lattice.

Silicon nitride

Silicon nitride (Si_3N_4) is polymorphic and therefore exists in several phases. Hexagonalα and β , amorphous, and also a high pressure, high temperature cubic polymorph. Si_3N_4 has excellent thermal chock resistance due to its low thermal expansion coefficient, and this property together with its high hardness of roughly 25 GPa makes Si_3N_4 suitable for wear resistance coatings. Other areas of use for Si_3N_4 is within electronics, e.g. as diffusion barriers in semiconductors and as an insulator layer. Within the amorphous Si_3N_4network the Si-N distance is 1.74 Å, and each silicon atom is bonded to four nitrogen atoms. The melting temperature of Si_3N_4 is 1900°C and the density 3.2 g/cm^3 [2].

3 FORMULATION OF PROBLEM

TiN has been widely used in protective hard coatings for bearings, gears, and cutting tools to prolong their service lifetime and improve cutting performance. However, TiN coatings predominantly grow with a columnar grain structure, and the columnar grain boundaries become sites for crack initiation, resulting in premature failure of TiN coatings.

Another evident drawback of TiN coatings is their limited oxidation resistance at high temperatures that can be reached during cutting processes. TiN starts to oxidize severely at temperatures as low as 500°C. Recently, S. Veprek [8] developed a new concept for producing superhard nanocomposite materials, which involves the preparation of a two-phase system, composed of a nanocrystalline hard material embedded in an amorphous matrix with strong interfaces between the two phases.

The most studied system up to now, and which revealed the most promising results, is the (Ti, Si) N system [1-5]. These films were characterized as nanocomposites consisting of TiN nanocrystallites embedded in amorphous Si_3N_4 matrix (nc-TiN/a-Si_3N_4), with a super hardness (> 40 GPa). These TiN/a- Si_3N_4 composites have also been shown to be thermodynamically stable and resistant to oxidation in air at temperatures up to 800°C.

Initially, the superhard nanocomposite coatings were synthesized by plasma enhanced chemical vapour deposition processes at 550-600°C .The gases ($TiCl_4$, $SiCl_4$ or SiH_4) used in CVD processes may pose problems in production because of their corrosive nature. Moreover, for most applications, a low deposition temperature is required to prevent substrate distortion and loss of mechanical properties.

Currently, significant effort is devoted to preparation of nanocomposite coatings using reactive magnetron sputtering, since this technology is a low-temperature and far less dangerous method compared to CVD. Also, it can be easily scaled up for industrial

applications. By using reactive magnetron sputtering, with DC power supplied, Ti-Si-N coatings with improved hardness and oxidation resistance compared to TiN have been reported by several research groups[6].

Due to the limited conductivity of silicon, positive charge can accumulate, and as a consequence arc may occur, on the target surface during DC sputtering, which in turn influences the coating quality. To minimize the charging effect, L. Rebouta et al. [5] connected a pulsed voltage signal onto the silicon target during their deposition of TiN/SiN_x multilayer coatings. In the present report, Ti-Si-N nanocomposite coatings were deposited by a magnetron sputtering, in which Ti and Si targets were sputtered by DC and RF power, respectively.

4 EXPERIMENTAL SETUP AND PROCEDURE

4.1 THE SPUTTERING SYSTEM

The system used for deposition was unbalanced magnetron sputtering system. Figure 4.1 shows the photograph of the system. It has various components, which are discussed below.

1. *Vacuum chamber:*

The chamber consists of substrate holder, sputtering guns, and heater. The substrate holder has an inbuilt substrate heater. This is connected to a thermocouple to measure the temperature and ensure proper control and monitoring of the substrate temperature. The system consists of two sputtering guns, which was used for co-deposition. The sputtering guns (diameter = 2 inches) had planar magnetron geometry. The sputtering guns are connected to power supplies.

2. *Rotary pump:*

It consists of a stator and an eccentric rotor with two vanes and a top seal. The inlet port is connected to the vacuum system and the exhaust port with the valve. This pump was operated to bring down the pressure to about $1 \dot{x} 10^{-3}$ torr.

3. *Turbo pump:*

This pump can further reduce the pressure inside the vacuum chamber to around 1×10^{-8} torr. Before deposition, the chamber was pumped down to a pressure of 4×10^{-6} torr using this pump.

4. Pressure Gauge:

This measures the pressure created by the rotary pump. It consists of a Wheatstone's bridge circuit with a filament made of a metal with a high temperature coefficient of resistance. The electrical resistance is directly proportional to the temperature. Gas molecules collide with the wire and remove heat. As gas molecules are removed, there are lesser collisions and hence the wire gets heated

up. Therefore resistance of the wire increases and this change in resistance is detected by the circuit.

5. Gas valve:

Gas valve is provided for constant flow of gases to sputtering chamber. Mainly mixtures of inert gases are uses in sputtering chamber. The gases may be argon, helium, nitrogen etc

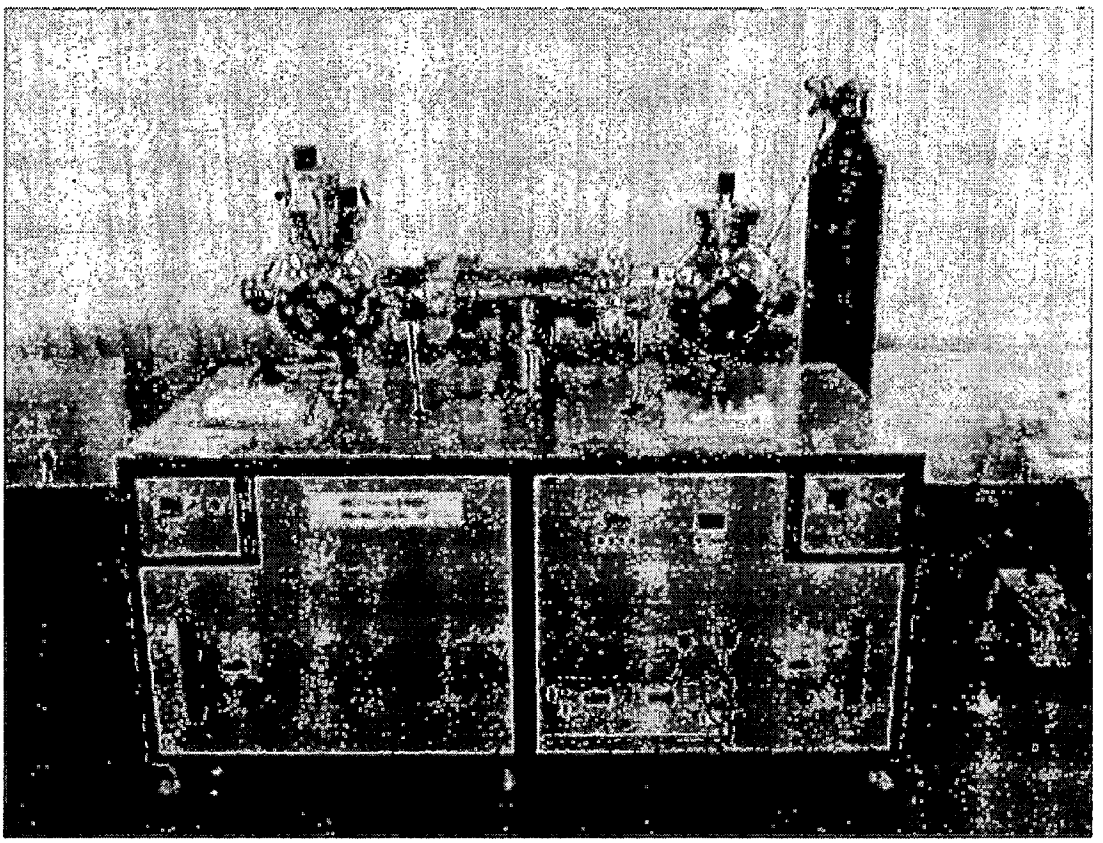

Fig.4.1Dual chamber sputtering system

4.2 PREPARATION OF SAMPLES

Silicon substrates were used for the deposition of TiN/ Si_3N_4 nanocomposite coatings. They were 5 mm x 10 mm and the orientation of the substrate was (100). Before placing inside the chamber, etching of silicon substrates was done using a mixture of hydrofluoric acid and nitric acid for 20 minutes so that the contaminants on the sample surfaces could be removed. Then they were subjected to ultrasonic cleaning using trichloroethylene, alcohol and acetone. The samples were then dried and placed inside the sputtering chamber.

4.3 GENERAL POINTS FOR IMPROVING PERFORMANCE

1 Cleanliness:-

• Clean the sputter chamber with hot soapy water and dry thoroughly, solvents can be used but we have found this unnecessary and having greater danger to health and safety. If the deposit is stubborn, use a kitchen scouring pad such as the green scotch bright variety.

• Use Isopropyl alcohol on metal surfaces, not Acetone which has greater danger to health and safety, it will also take longer to out gas and reduce the vacuum performance.

Vacuum:-

Never leave the chamber under vacuum without isolating the roughing pump from the coater, this must be done with a manual valve. Failure to do so will increase suck back of Hydrocarbons (pump oil) in to the sputter chamber and increase contamination.

• Always ensure the system is dry and pumping to its correct vacuum level before working with samples, failure to do so will result in poor sputter rate and contamination.

3. Sputter gas:-

Always use high purity Argon gas of the grade known as "White spot" this will ensure fast sputter rate and good pump down time.

4.4 EXPERIMENTAL PROCEDURE

Titanium silicon nitride ($Ti_{1-x}Si_xN$) films were deposited by IMSD, using separate Ti (99.96%) and Si (99.999%) dc magnetron targets (55 mm diameter x 5 mm thickness). Film stoichiometry, Ti_{1-x}: Si_x (where x is the atomic fraction of Si: x = Si / [Ti + Si]) could be precisely controlled with the power to each target. The target power density was typically set at 5.2 W/cm^2 for Ti and Si power density was varied (1.55-2.60 W/cm^2). The base pressure of the deposition chamber was10^{-8} Pa, and the depositions were carried out in 1.4 Pa Ar/N2(50:50): the gases both of 99.9999% purity were pre-mixed in a reservoir and bled into the system via a gas valve. By setting the gas valve and gate valve to the main pump, gas flow rate and pressure were controlled. The target to substrate distance was fixed at 40 mm. The Substrates rested on a heater. The heater temperature was measured with optical pyrometer .The dc substrate bias was varied over the range of 0 to −200V. Targets were pre-sputtered for 15 min prior to film growth, with a shutter placed in front of substrates [30].

Chemically cleaned substrates were dried and then subjected to glow discharge cleaning in the vacuum chamber. The plasma cleaning of the substrates was done for about 5 minutes by bombarding Ar^+ on the substrate using a substrate bias of -200 V.

Argon flow rate of 20 sccm for the chamber. After substrate cleaning, target cleaning was done for about 5 minutes. Before deposition of the film, about 0.5 μm thick titanium interlayer was deposited to enhance the adhesion between the coating and the substrate surface. After deposition of the interlayer, the nitrogen flow was turned on and a bias voltage of -200 V was applied to the substrate for the deposition of TiN/Si_3N_4. The various parameters for deposition are given below:

Base Pressure (P_B)		10^{-8} Pa
Substrate heating	Temperature	400 ^{0}C
	Time	30 min
Substrate cleaning with bias	Voltage bias(V_B)	-200 V
	Argon gas flow	20 sccm
	Time	5 min
Target cleaning	Time	5 min
Nanocomposite coating	Coating pressure (P_C)	1.4 Pa
	Voltage bias(V_B)	-200 V
	Argon gas flow	20 sccm
	Nitrogen gas flow	20sccm
	Temperature	800 ^{0}C
	Time	3 min

4.5 EXPERIMENTAL RESULTS

Table 4.1 Effect of bias voltage

Sample No.	Substrate Bias(V)	Hardness(Gpa)
1.	20	22.1
2.	80	23.64
3.	150	32.75
4.	200	26.95

Table 4.2 Effect of Temperature

Sample No.	Temperature (^{o}C)	Hardness(Gpa)
5.	800	23.87
6.	850	25.26
7.	900	28.06
8.	1000	30.12

Table 4.3 Effect of silicon content

Sample No.	Si content (%)	Hardness(Gpa)
9.	8	32.21
10.	16	29.84
11.	20	30.96
12.	23	31.39

5 TECHNIQUES FOR CHARACTERIZATION OF THE NANOCOMPOSITE COATINGS

5.1 X-RAY DIFFRACTION

X-ray diffraction is a powerful analytical technique which is widely used in many fields of science and in many industries for applications ranging from basic research to routine quality control, structural characterization. It is used to identify new compounds and crystalline structures, to identify unknown materials in terms of its crystalline structure, and to look for deviations from the perfect structure which may indicate the presence of impurities, strain, the size of the crystals and other fine-scale structural defects.

The principle behind this technique relies on the constructive and destructive interference of x-rays emitted from a sample that had been illuminated by a filtered and focused x-ray beam. If certain conditions are met then the intensity of these x-rays will be strong. These conditions tell us about the spacing between planes of atoms in the crystal structure as well as a host of other details.

In X-ray diffraction , when a monochromatic X-Ray beam with wavelength λ is projected onto a crystalline material at an angle θ, diffraction occurs only when the distance traveled by the rays reflected from successive planes differs by an integral number of wavelengths, n. If the lattice spacing is d, diffraction peaks will be observed at angles θ satisfying Bragg's equation 5.1 . Plotting the angular positions and intensities of the resultant diffracted peaks of radiation produces a pattern, which is characteristic of the sample. The Bragg's equation is:

$$2d \sin\theta = n\lambda \qquad \text{----------5.1}$$

The width of the diffraction peaks in a particular pattern provides an indication of the average crystallite size. Large crystallites give rise to sharp peaks, while the peak width increases as crystallite size reduces. X-Ray diffraction can be classified into two categories: low angle ($2\theta \leq 15$) and high angle ($2\theta \geq 15$).

The distinction is made because low angle X-Ray diffraction results from the reflection of X-Rays off the interfaces between layers, while high angle diffraction results from diffraction of X-Rays off individual atom planes in the superlattice. In our experiment, the XRD data of the films were recorded in a Rigaku D/max 2200-powder diffractometer. The X-Ray source was a CuK_{α} radiation (λ = 1.5418 Å). The crystallite size of the coating can be determined using the Debye-Scherrer formula,

$$L = \frac{0.94\lambda}{\delta \cos(\theta)} \quad \text{----------5.2}$$

Where, λ is the wavelength of the X-Ray,δ is the FWHM (Full Width at Half Maximum) of the reflection andθ is the Bragg's angle [31].

5.2 ATOMIC FORCE MICROSCOPY

An atomic force microscopy (AFM) maps out the topography of the surface by sensing the forces of interaction between the atoms belonging to the sample surface and the ones on tip of the probe. Fig shows the basic components of the AFM. To image the surface features, the sample is scanned by an atomically sharp tip, usually made of Si or Si_3N_4, attached to lower side of reflective cantilever. Light from a diode laser is focused on the cantilever and is reflected on to a dual element photo- diode. As the sample is scanned below the tip, the cantilever moves up & down which change the ratio of light falling on the two elements of photo–diode. The difference in intensity falling on two elements is converted into a proportional voltage by photodiode. This voltage serves as a feedback signal enabling the tip to maintain either a constant force or a constant height above sample. For most of the applications the instrument is operated in one of the following three modes:

1. Contact mode:

In this mode, the tip is kept in contact with the surface. The repulsive force between the sample atoms and the tip atoms (10^{-9} N) is transmitted by a piezoelectric crystal onto the cantilever. If the deflection of the cantilever ids different

than some pre-set value, then the feedback amplifier applies a voltage to the piezo to raise or lower the sample relative to cantilever to restore the desired value of deflection. The voltage applied to the piezo is measure of the height of the feature on the sample surface. The typical problem with the contact mode is that the tip may scratch the surface and change its intrinsic features.

2. Non- contact mode:

In this mode, the tip is held at 50 to 100 ^{o}A above the sample surface. The interaction between the tip and the sample is due to attractive Van-der Waals forces. Since these forces are much weaker than the repulsive forces in the contact mod, an AC technique is used for their detection. The tip is vibrated and the change in the oscillation frequency, amplitude, or the phase in response to force gradient is monitored.

3. Tapping mode

Tapping mode is a key advance in AFM. This potent technique allows high resolution topographic imaging of sample surfaces that are easily damaged, loosely hold to their substrate, or difficult to image by other AFM techniques. Tapping mode overcomes problems associated with friction, adhesion, electrostatic forces, and other difficulties that an plague conventional AFM scanning methods by alternately placing the tip in contact with the surface to provide high resolution and then lifting the tip off the surface to avoid dragging the tip across the surface. Tapping mode imaging is implemented in ambient air by oscillating the cantilever assembly at or near the cantilever's resonant frequency using a piezoelectric crystal. The piezo motion causes the cantilever to oscillate with a high amplitude (typically greater than 20nm) when the tip is not in contact with the surface. The oscillating tip is then moved toward the surface until it begins to lightly touch, or tap the surface. During scanning, the vertically oscillating tip alternately contacts the surface and lifts off, generally at a frequency of 50,000 to 500,000 cycles per second. As the oscillating cantilever begins to intermittently contact the surface, the cantilever oscillation is necessarily reduced due to energy loss caused by the tip contacting the surface. The reduction in oscillation amplitude is used to identify and measure surface features [30].

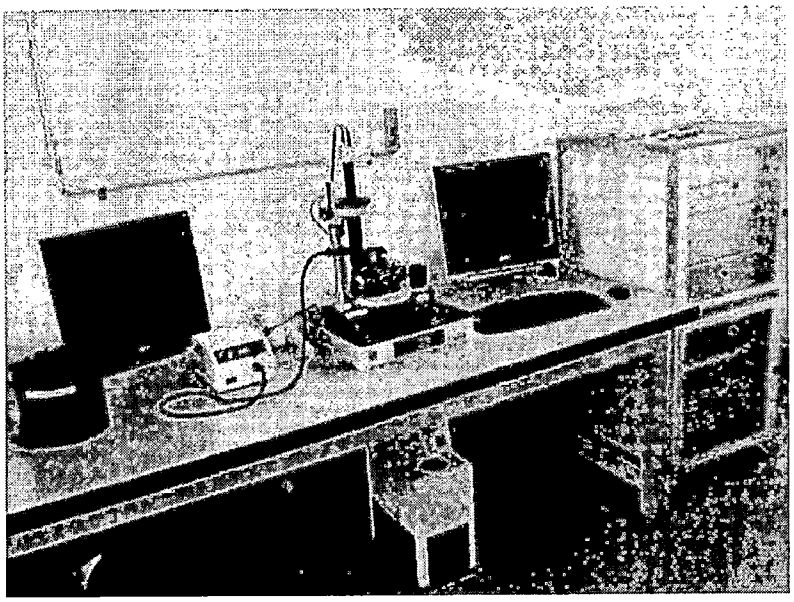

Fig 5.2 Atomic force microscope

5.3 NANOHARDNESS TESTING

Nanoindentation is a technique in which continuous measurement of force and displacement is carried out, while an indenter of known geometry is pressed into the sample material. The nanohardness tester consists of two distinct components, a measuring head for performing indentation and an optical microscope for selecting a specific sample location prior to the indentation and for checking the location of the imprint after indentation. Both components are directly linked by a positioning system, which allows movements in X-Y axes. The main advantage of this instrument is its differential measurement of the sample surface made possible by a sapphire reference ring, which remains in contact with the sample during the loading and unloading cycle, thus giving exact position of the indenter tip relative to the sample surface. The samples were kept under optical microscope and a suitable area was chosen. Indentations were made on the desired area using a Berkovich diamond indenter. Several indentations were made so as to improve the accuracy of the measurements. After initial contact of the indenter on surface, the load was increased at a redetermined rate and then decreased at the same rate to zero. For all the samples, the maximum applied load was 10 mN. For each loading and unloading cycle, the load was

plotted against the displacement of the indenter. From the load vs. displacement plot, hardness (H) was calculated using the method of Oliver and Pharr (1992) according to the relation 5.3,

$$H = Pmax / A \qquad \text{---------- } 5.3$$

Where, Pmax is the peak indentation load and A, the indentation contact area. The loading curve provides the hardness of the coating and the unloading curve provides the elastic modulus of the coating. Smaller the indentation depth, higher is the hardness [17].

6 RESULT & DISCUSSION

6.1 EFFECT OF SUBSTRATE BIAS

Fig.6.1 shows XRD spectra of the $Ti_{1-x}Si_xN$ films deposited at 400 ^{0}C with varying negative substrate bias voltages, *V*b, from −20, to−200V. These observations are in agreement with earlier findings [22] from nc-TiN/*a*-Si_3N_4 films deposited by magnetron sputering , suggesting that the silicon is present in an amorphous phase. The undoped TiN film shows strong preferred (1 1 1) orientation and a narrow line width corresponding to a grain size of approximately 30 nm. For the $Ti_{1-x}Si_xN$ films, an increase in negative substrate bias gradually changes the preferred film orientation of TiN (in $Ti_{1-x}Si_xN$) from (1 1 1) to mixed, and finally to (2 0 0), with broadening of the peaks. Peak broadening is generally attributed to reduction in the coherent diffracting domain size (related to grain size) and/or microstrains due to defects.

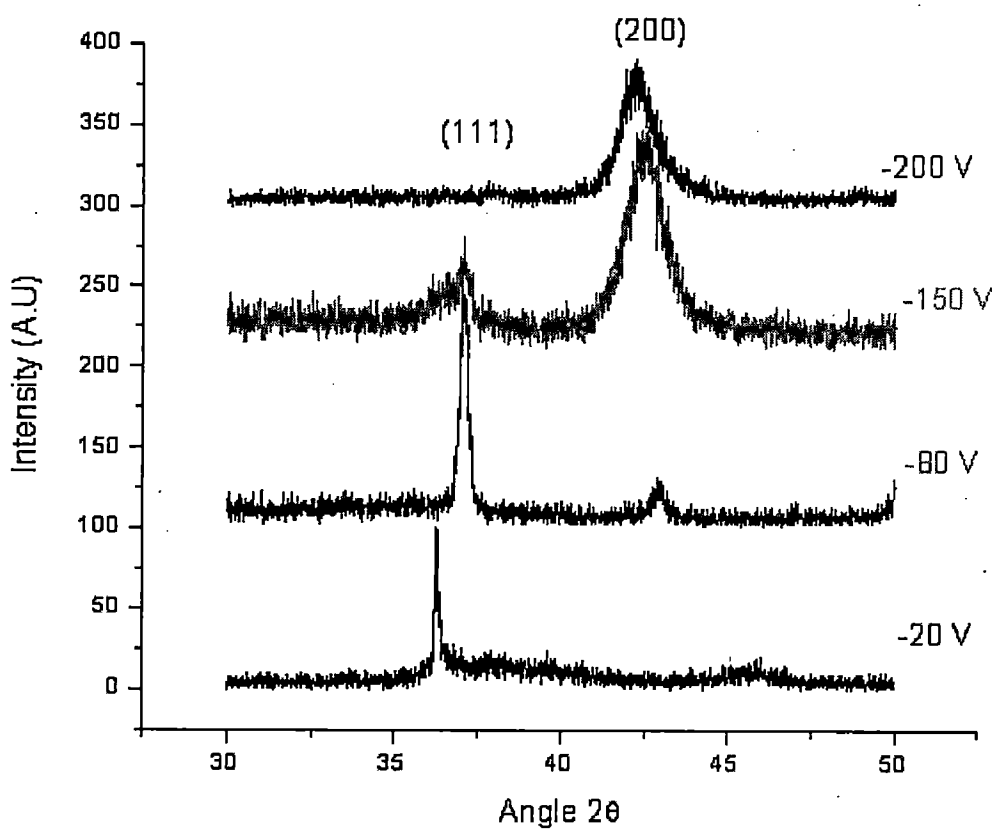

Fig 6.1 XRD patterns of $Ti_{1-x}Si_xN$ films deposited at various substrate bias voltages

The negative bias on the substrate influences ion bombardment parameters (momentum, kinetic energy etc.) and hence the microstructure of the growing film. As shown in Fig.6.1, the preferred orientation of TiN (1 1 1) changes to (2 0 0) orientation with increase in negative bias from −20 to −200V. Similar changes in film orientation have also been observed by varying other processing parameters e.g. nature of the sputtering gas in earlier references [30]. Generally, the (1 1 1) plane in the TiN crystal has the lowest strain energy, while the (2 0 0) plane has the lowest surface energy. It is assumed that the growing coating develops a crystallographic texture in order to minimize the total energy of the system.

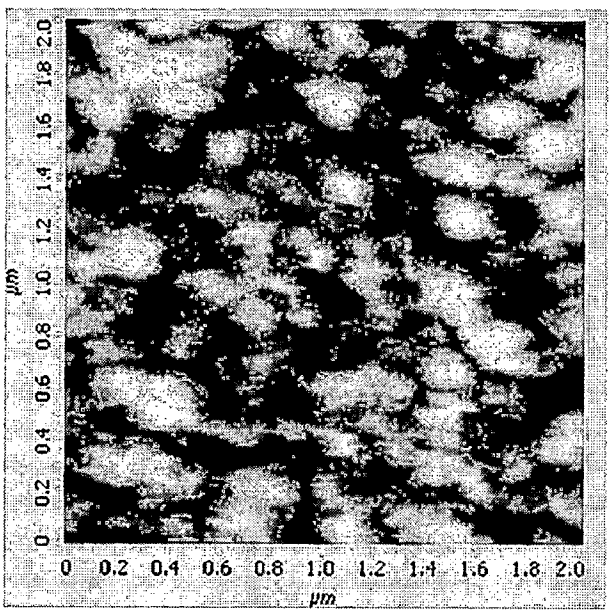

Vb = -20V

Fig 6.2 (a) AFM Image of Ti–Si –N at substrate bias Vb = -20V

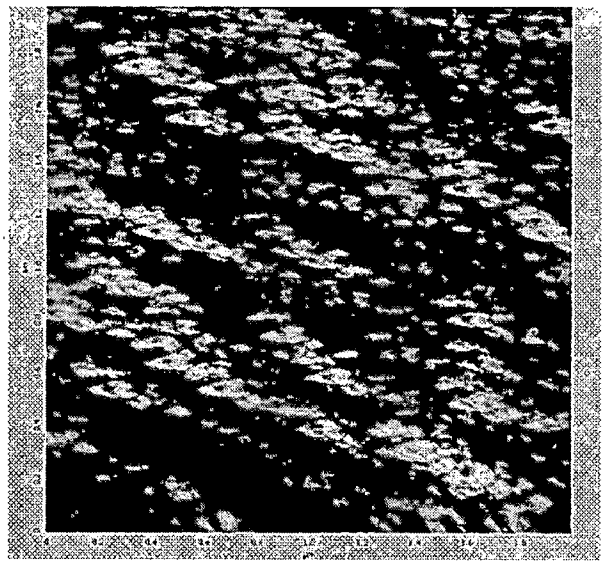

Vb= -80V

Fig 6.2 (b) AFM Image of Ti–Si –N at substrate bias Vb = -80V

Vb = -150 V

Fig 6.2 (c) AFM Image of Ti–Si –N at substrate bias Vb = -150V

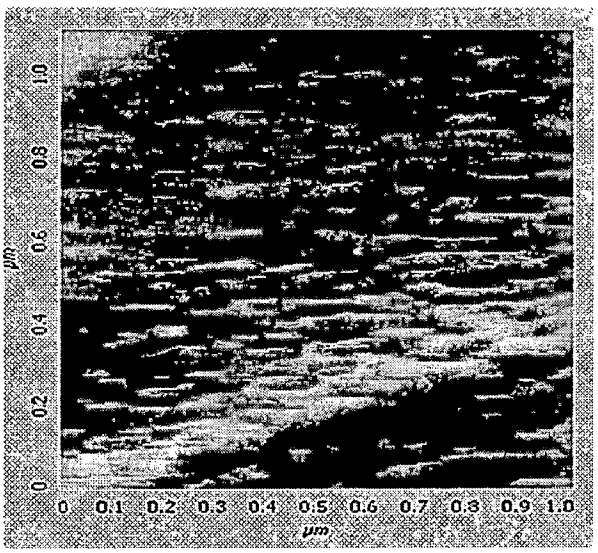

Vb = -200V

Fig 6.2(d) AFM Image of Ti–Si –N at substrate bias Vb = -200V

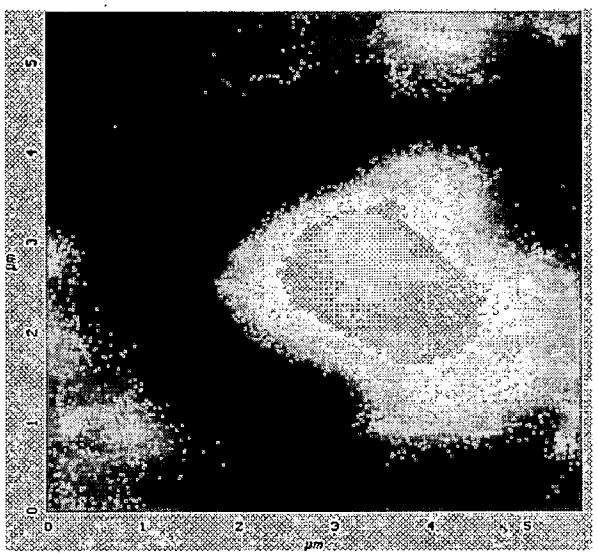

Vb= -200V

Fig 5.2 (e) AFM Image of Ti–Si –N at substrate bias Vb = -200V

The addition of silicon changes the surface morphology of deposited films from a pronounced columnar microstructure with faceted grains to a dense, fine grained structure. Figures 5.2 (a-e) shows the AFM images of the films deposited at varying negative substrate bias voltages *V*b (−20, −80, −150 and −200 V), The effect of increasing the bias voltage, *V*b from −20 to −200V results in decrease of grain size as observed in AFM images. In general with increase in negative substrate bias the energy of the incident ions increases that leads to increase in the grain size because of the

increase of adatom mobility. However in our case due to the presence of amorphous matrix of Si_3N_4, the grain growth of TiN phase is suppressed resulting in more surface defects and consequently a higher density of nucleation sites on the substrate. The surface roughness of $Ti_{1-x}Si_xN$ films is also affected by the negative substrate bias during deposition. A decrease in surface roughness upon increasing negative substrate bias has been observed as shown in Fig. 6.2(b and c) [at Vb = −80V (RMS, 2.55 nm), and at Vb = −150V (RMS 1.35 nm respectively)]. The increase in Vb above −150V results in the increase of surface roughness due to re-sputtering of the growing film. Although the surface roughness of the films deposited at Vb −200V at a scale of μm is very small (RMS, 0.548 nm) with a very small crystallite size (≈5 nm), however overall surface of the films at mm scale becomes very rough leading to deterioration of mechanical properties. This result could be explained by the XRD results of Fig 6. 1 From XRD patterns, the peak broadening, indicating the size reduction of TiN (30 nm for (Vb = - 20 V); 18–20 nm (Vb = −80 V), 10 nm (Vb = −150 V) and 5 nm (Vb = −200 V) of $Ti_{1-x}Si_xN$films), and the microstructure changes from strong (1 1 1) preferred orientation to mixed one and finally to highly (2 0 0) orientation with increase in substrate bias voltage. It is understood that surface roughness is related with the size and orientation of TiN crystallite and is well known that the increase of Vb leads to the enhancement of the adatom surface mobility as well as the atomic diffusion, thereby enhancing grain growth, which contributes to the increase of grain size and surface roughness But the presence of the amorphous matrix of Si_3N_4, suppresses the grain growth of TiN nanocrystals, leading to a finely grained dense microstructure.

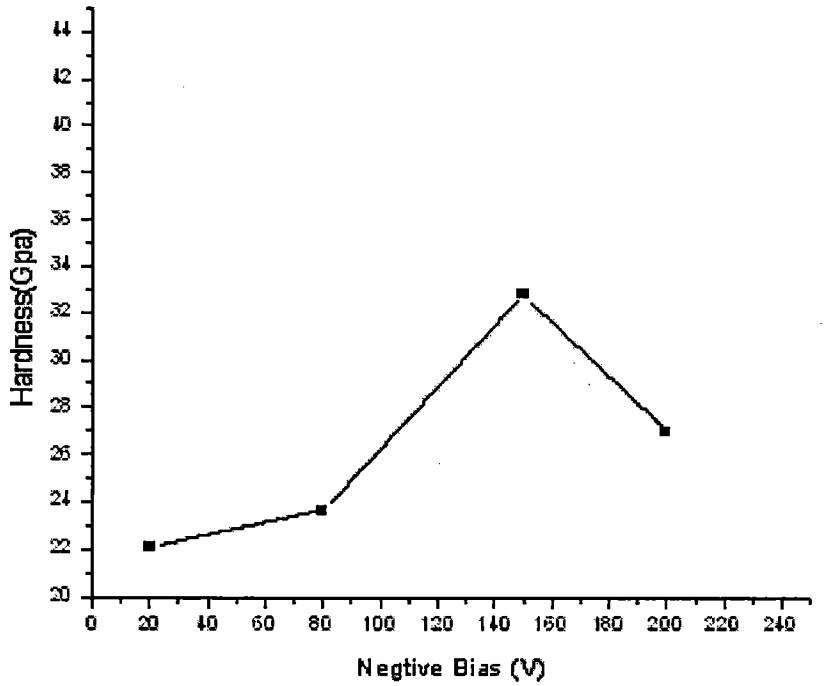

Fig 6.3 Hardness values of $Ti_{1-x}Si_xN$ films as a function of negative substrate bias voltage.

Fig. 6.3 shows hardness, *H*, of $Ti_{1-x}Si_xN$ films as a function of substrate bias (*V*b). The hardness of the films increases with increasing negative bias *V*b, and reached a maximum value of 40 GPa at −150V and dropped again with further increase in *V*b. Above dc bias of −150V, the resputtering of the growing film by bombardment of energetic particles results in large surface roughness and hence a decrease in hardness value. The high hardness value is attributed to the nanocomposite structure described by Veprek [32] that leads to change in grain size, orientation, and increase in density and elimination of voids. All these effects are related to the adatom mobility and the ion–solid interactions near the growing film surface under negative bias. The increase in *V*b increases the mobility of adatoms promoting closed packed structure in near thermodynamic equilibrium conditions. Thus, for high adatom mobility $Ti_{1-x}Si_xN$ films are expected to grow along the (2 0 0) orientation corresponding to the lowest surface free energy . On the other hand, for low adatom mobility the preferred orientation is the (1 1 1) in which the highest number of atoms per unit area can be incorporated at low energy sites. The

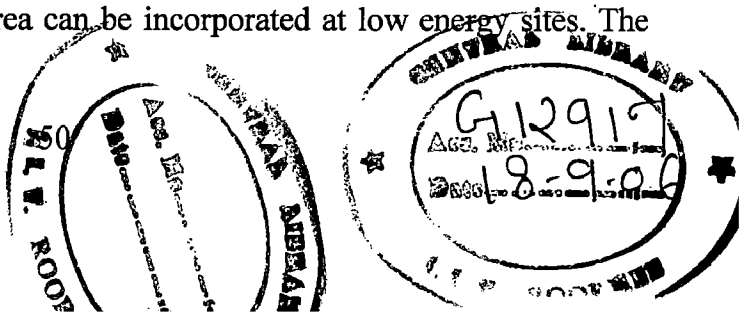

amounts of grains grown along the (2 0 0) and (1 1 1) orientations play a significant role on the mechanical properties of $Ti_{1-x}Si_xN$ films. The crystallite size showed a monotonous decrease with increasing Vb, but the maximum hardness was obtained for a Vb = −150V. We have observed that in addition to the decrease in grain size, the negative bias of the substrate during deposition strongly influences the preferred orientation of the reactively sputtered $Ti_{1-x}Si_xN$ films. Development of a preferred orientation in non-epitaxial thin films (where the substrate plays a relatively minor role in the texture determining process) is primarily governed by the surface and strain energy considerations. Thermodynamics drives the system towards the minimum possible sum of surface and strain energies under the restrictions imposed by kinetics. In TiN (2 0 0) planes or the square surfaces of the cubic unit cell have the lowest surface energy [33]. The increase in Vb increases the energy of the atoms to diffuse on the substrate surface. Thus, the adatoms are no longer kinetically constrained to metastable high-energy configurations, but relax to the lowest surface energy configurations of (2 0 0) planes. However due to much higher kinetic energy imparted due to large negative substrate bias (−200 V) leads to re-sputtering of the deposited film leading to deterioration of surface and hence the mechanical properties.

6.2 EFFECT OF SILICON CONCENTRATION

The reason for the superhard Ti–Si–N coatings compared to TiN coatings has been reported due to its microstructural changes. For instance, nanograin size and a randomly oriented microstructure should be especially attributed to its superhigh microhardness, i.e., hardening by grain-size refinement, which is well understood in terms of the Hall–Petch model. In addition, the multioriented grain structure of Ti–Si–N coatings can also enhance mechanical strength by inhibiting the dislocation propagation to adjacent grain, Another possible role for amorphous Si_3N_4 is prohibiting dislocation movement by the pining effect, thus causing an increase in microhardness. The decrease of microhardness with the further increase of Si content is probably due to the coarsening of the microstructure of Ti–Si–N coatings.

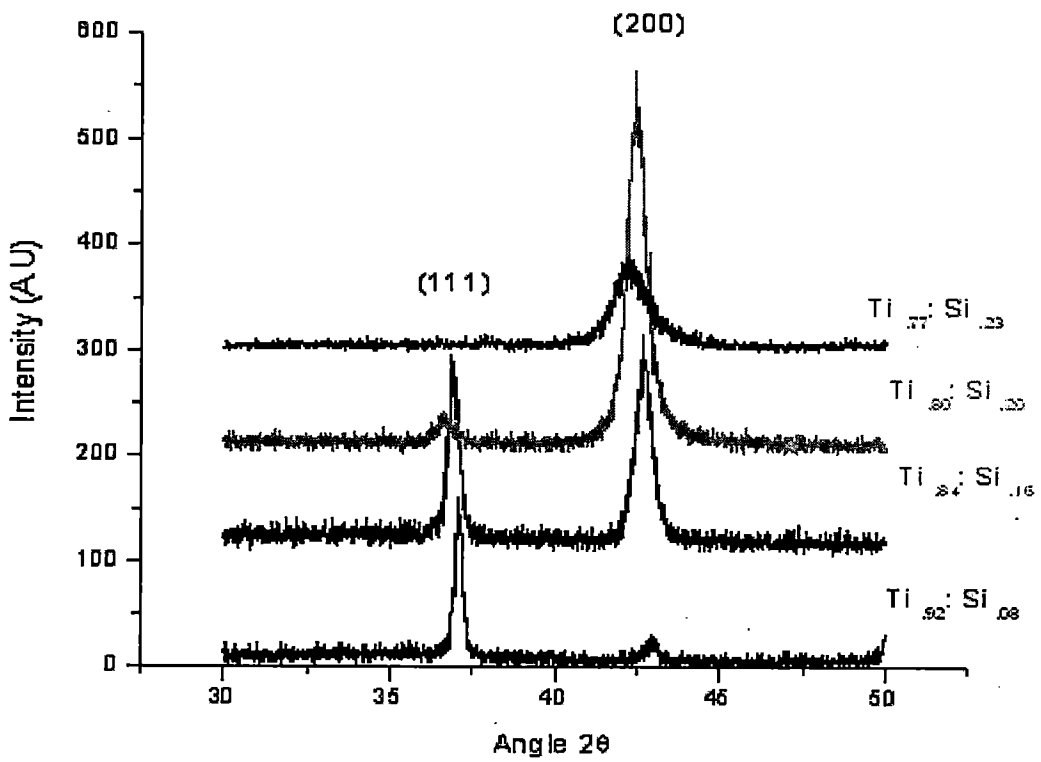

Fig 6.4 XRD spectra of nc-TiN/a-SiN $_x$ films with varying Si content

The X-Ray diffraction patterns of TiN/ Si_3N_4 films deposited on silicon substrates at various silicon concentrations (a) 8% (b) 16 % (c) 20 % (d) 23 % are shown in Figure 6.4 .

In the XRD patterns of Ti–Si–N coatings deposited at varying silicon content as shown in Fig 6.4 show that Ti–Si–N coating have a strongly preferred TiN (111) orientation at lower Si content 8 at. % Si. Furthermore, no new crystalline phases are detected except TiN, but the intensity peaks of TiN seem to broaden. This implies, to some extent, that the crystallite sizes in the coatings have been reduced. However, the Ti–Si–N coatings have somewhat mixed orientations of (111), (200) with increasing silicon content .

For silicon contents ≥ 16 %, there was an increase in the peak width corresponding to the (200) reflection and most of the crystals were oriented along the (200) plane or we see that the intensity of the (111) peak decreases with increase Si percentage.

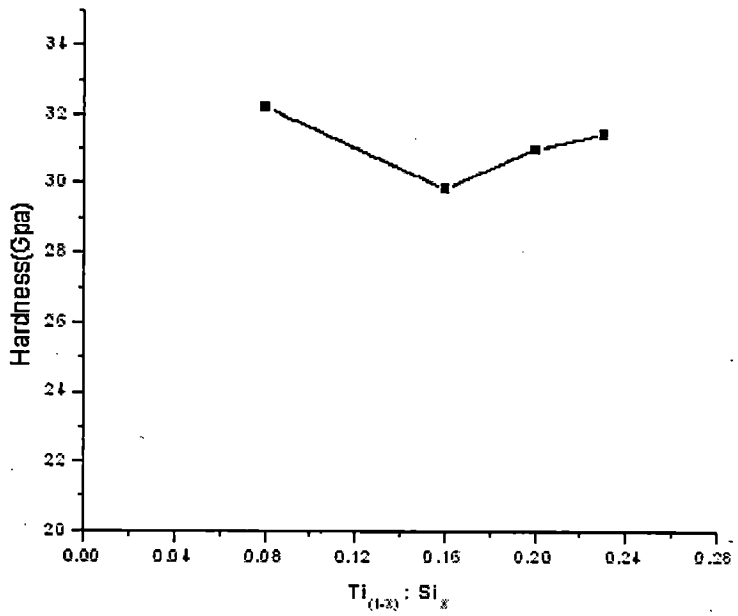

Fig 6.5 Relationship between hardness and Si content in Ti-Si-N Films

We have also noted that the hardness of the Ti-Si-N coatings is a distinct function of Si content. With lower Si incorporation, the hardness enhancement could be ascribed

to the hindrance effect of the segregated Si_3N_4 on TiN grain boundary sliding which is the predominant deformation mechanism in nanocrystalline materials. With increasing Si content, more and more TiN grain boundaries would be covered with the amorphous Si_3N_4, and the hindrance effect on grain boundary sliding became more significant. As a consequence, the coating hardness would increase with increasing Si content. When Si incorporation exceeds a certain level, however, the amorphous Si_3N_4 components will make a contribution to the overall hardness of the Ti-Si- N coatings. In the above figure with increase in silicon content hardness is increasing due to grain size refinement.

We also see this effect through AFM images shown in figure 6.6(a-b). The AFM shown in figure 6.6(a) shows that films composed of nanocrystalline (nc) TiN embedded in an amorphous silicon nitride (a-SiN_X) matrix.

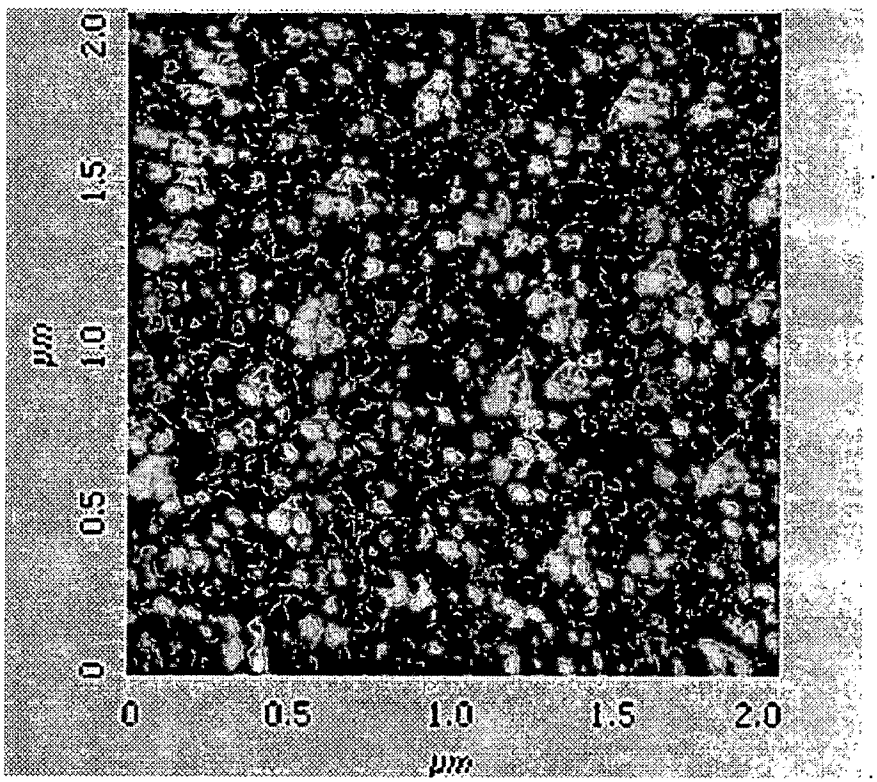

Fig 6.6(a) AFM Image of Ti–Si –N at Silicon content 0 ·23%

The surface morphology of the coatings was studied using Atomic Force Microscopy. The 3-D AFM image of TiN coating and TiN/Si_3N_4 nanocomposite coating are shown in Figure 6.6(b). The average roughness was 17.47 nm for TiN whereas for TiN/Si_3N_4, it was 8.22 nm. This decrease in roughness can be attributed to the smaller crystal size in the case of the nanocomposite coating. The deposited coatings showed no granular features indicating that the coatings were smooth.

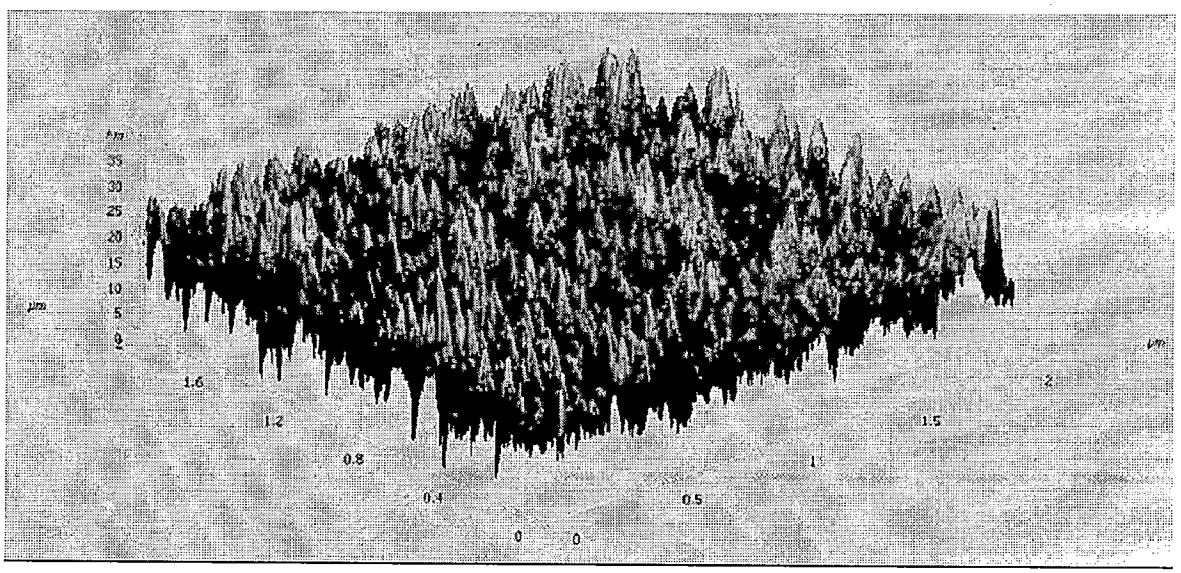

Fig 6.6 (b) 3-D AFM image of Ti-Si-N coating

6.3 EFFECT OF DEPOSITION TEMPERATURE

As has already been mentioned above, unique properties of the nanocomposite films are due to their nanostructure. The nanostructure is, however, a metastable phase. This means, if the temperature under which the film is operated overpasses some threshold value T_{cr} (critical temperature) the material of the film starts to crystallize. It results in a destruction of the nanostructure and/or the formation of new crystalline phases. This is a reason, why the nanocomposite films lose their unique properties at temperatures T_{cr}. Simply said, the temperature T_{cr},at which the nanostructure converts into large grains and-or a new crystalline phase, determines the thermal stability of the nanocomposite. Many applications, however, require T_{cr} to be higher than 700 ^{0}C. Therefore, it is vitally important to develop new materials which will be thermally stable against crystallization and oxidation at temperatures T considerably exceeding 700 ^{0}C .

In order to test the thermal stability of the coatings, TiN/ Si_3N_4 films were heated in a furnace. The structural changes as a result of heating were characterized using XRD and nanoindentation. The results indicated that TiN/ Si_3N_4 films were stable up to 800°C compared to TiN films, which got oxidized at 500°C .

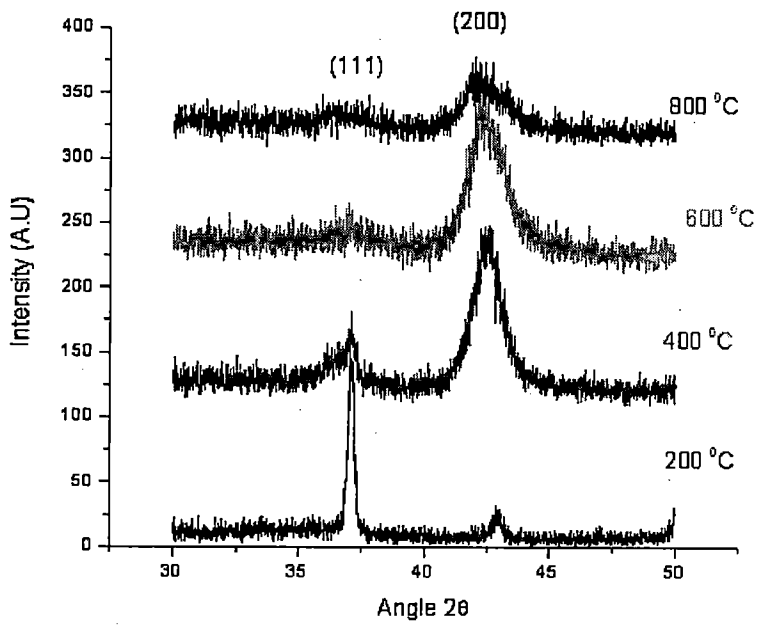

Fig 6.7 XRD scans of Ti-Si-N films at varying deposition temperature

Fig.6.7 shows a series of XRD patterns of the coating layers at various deposition temperatures. At 200 ^{0}C, the peaks corresponding to the TiN (111) and (200) crystal planes were observed. Typical XRD patterns for Ti–Si–N film having multi-oriented microstructures appeared at deposition temperatures of 200 and 400 ^{0}C, but it changed to a strong (200) preferred orientation above 600 ^{0}C.

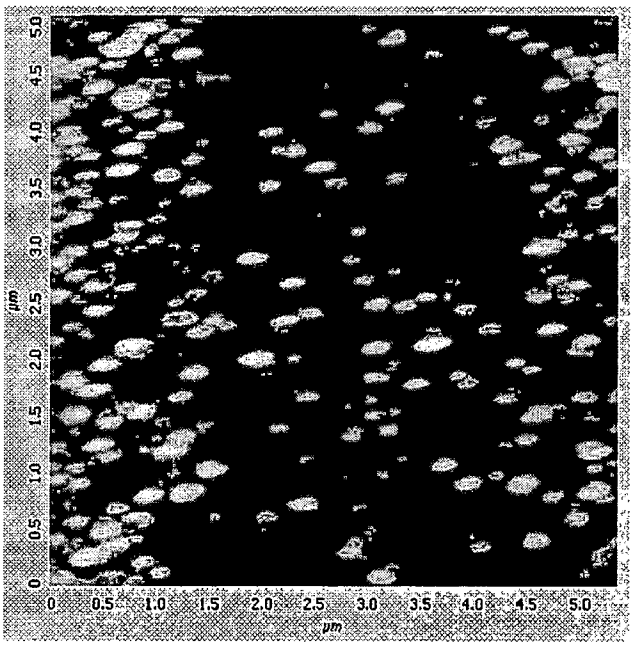

Fig 6.8 (a) AFM image at temp 800 ^{0}C

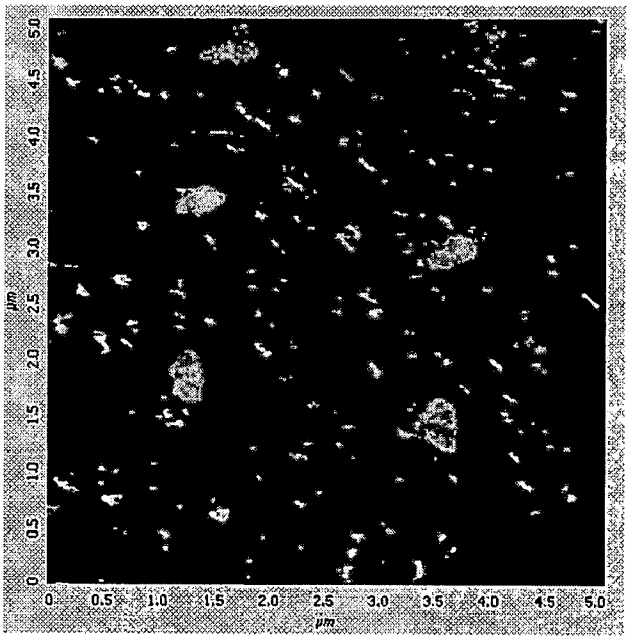

Fig 6.8 (b) AFM image at temp 400 ^{0}C

The microstructural change of Ti–Si–N coating layer with deposition temperature is shown again in AFM images of Fig. 6.8(a, b). Fig. 6.8(a) of AFM shows that the Ti–Si–N coating layer was grown with dense and fine grain structure above 800 ^{0} C. On the other hand, the coating layer deposited below 400 ^{0} C showed a columnar structure with large grain size (Fig 6.8(b)), and had a poor crystallinity due to insufficient thermal energy to decompose the reactants. The relatively low microhardness of coating layers deposited below 400 ^{0}C seemed to be strongly related to these microstructures.

The figure 6.9 represents microhardness of Ti–Si–N coatings with variations in deposition temperature. The coating layers had the highest microhardness, approximately 31 Gpa at 800 ^{0}C and the microhardness increased as the temperature increased above 600 ^{0}C.

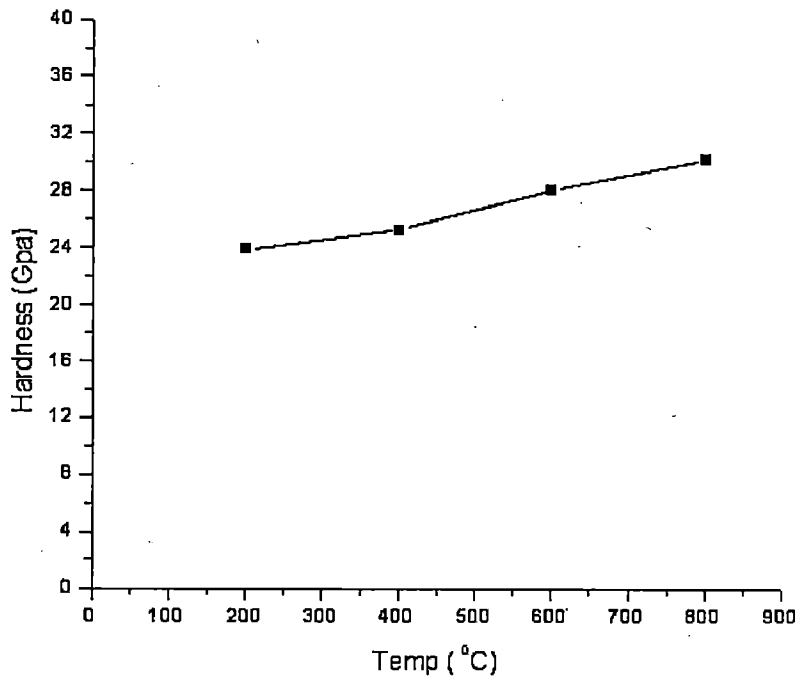

Fig 6.9 Hardness value as a function of deposited temperature

7 CONCLUSIONS AND SUGGESTION FOR FUTURE RESEARCH

This work has demonstrated the ability to deposit nanocomposite Ti-Si-N films using the ions assisted magnetron sputtering deposition (IMSD) technique. The results show the effects of ion flux and energetic bombardment on the properties of the films. Ion bombardment influences the texture, structure, and crystallite domain size, and therefore the mechanical properties of the films. XRD analysis indicates the formation of an amorphous phase and nanocrystalline TiN.

Nanocomposite thin films of $Ti_{1-X}Si_XN$ were deposited on Si substrates using ionized magnetron sputtering. The effect of processing parameters on the microstructure of these films was investigated using XRD and AFM. During deposition of the $Ti_{1-X}Si_XN$ films, the increase in negative bias voltage V_b, results in a structure change from (1 1 1) orientation with large TiN crystallite to (2 0 0) with a smaller size. The surface morphology of the films is also affected with increase in negative bias V_b. The roughness of the films is found to decrease with increase in V_b up to −150 V and with further increase in bias voltage to −200V, the surface roughness increases due to re-sputtering which leads to deterioration of the mechanical properties of $Ti_{1-X}Si_XN$ films .The best mechanical properties (H = 30-40 GPa) of the $Ti_{1-X}Si_X$ thin films for the present study were obtained at a negative dc substrate bias V_b of −150 V.

We also observe that the increments of hardness as the silicon contents were increasing without the effect of bias voltage. For silicon contents ≥16 %, there was an increase in the peak width corresponding to the (200) reflection and most of the crystals were oriented along the (200) plane or we see that the intensity of the (111) Peak decreases with increase Si percentage.

Hardness of Ti–Si–N coatings also varying with variations in deposition temperature. The coating layers had the highest microhardness, approximately 31 Gpa at 800 ^{0}C and the microhardness increased as the temperature increased above 600 ^{0}C.

Future work

Next activity in the field of nanostructured thin films will be concentrated mainly on the following problems: (1) the development of films with controlled size of grains in the range from 1 to 10 nm with the aim (a) to investigate size dependent phenomena in nanostructured films and (b) to develop new advanced coatings with unique physical and functional properties, (2) nanocrystallization from amorphous phase, (3) electronic charge transfer between nanograins with different chemical composition with the aim to produce films with new functional properties, (4) development of new nanostructured and nanocomposite coatings based on oxides and mixture of oxides and nitrides or carbides or other compounds (5) development of protective coatings with high oxidation resistance exceeding 2000°C, (6) low temperature deposition of crystalline nanostructured functional films on heated sensitive substrates such as polymer foils and polycarbonate, and (7) development of new PVD systems for the production of nanostructured coatings under new physical conditions and with high deposition rate. Also, it can expected that very soon thin nanostructured films will serve as experimental models for the design of nanostructured bulk materials with prescribed properties.

REFERENCES

[1] H. Gleiter, J. Material Science. 33 (1989) 223

[2] P.G. Sanders, J.G. Barker, J.R. Weertman, J. Mater. Res. 11 (1996) 311

[3] Y.K. Huang, A.A. Menovsky, F.R. de Boer, Nanostruct. Mater. 2 (1993) 505

[4] F. Vaz et al, "Young's modulus of (Ti,Si)N films by surface acoustic waves and indentation techniques", Thin Solid Films 408 (2002) 160-168

[5] L. Rebouta et al, "Hard nanocomposite Ti-Si-N coatings prepared by DC reactive magnetron sputtering", Surface and Coatings Technology 133-134 (2000) 234- 239

[6] J.Musil, "Hard and superhard nanocomposite coating", Surface and Coatings Technology 133-134 (2000) 322-330

[7] H. Jensen, J. Sobota, G. Sorensen, Surf. Coat. Technol. 94/ 95 (1997) 174

[8] J. Musil , F. Regent, J. Vac. Sci. Technol. A 16 (6) (1998) 3301

[9] C.G. Granqvist, R.A. Buhrman, J. Appl. Phys. 47 (1976) 2200

[10] H. Gleiter, in: N. Hansen, A. Horsewell, T. Lefferes, H. Lilholt (Eds.),"Deformation of Polycrystals: Mechanisms and Microstructures", Riso National laboratory, Roskilde, Denmark, 1981, pp. 15–21

[11] G. Gonzalez, J.A. Freites, C.E. Rojas, Scr. Mater. 44 (2001) 1883

[12] M.L. Hitchman, K.F. Jensen, "Chemical Vapor Deposition Principles and Applications", Academic Press, London,1993

[13] P .Sigmund ,"Theory of sputter yield of Amorphous and Polycrystalline Target", Phys. Rev. 184, 383 (1978)

[14] K.H. Kim, S.H. Lee, Thin Solid Films 283 (1996) 165

[15] W.H. Bragg, Phil. Mag. 27 (1914) 881

[16] S. Z. Li, Y. Shi and H. Peng, Plasma Chem. Plasma Process. 12 (1992) 287

[17] S. Veprek, S. Reiprich and S. Z. Li, Appl. Phys. Lett. 66 (1995) 2640

[18] S. Veprek and A. S. Argon, J. Vac. Sci. Technol. B 20 (2002) 650

[19] M. J. Demkowicz and A. S. Argon, Phys. Rev. Lett. 93 (2004) 025505

[20] S. Veprek and S. Reiprich, Thin Solid Films 268 (1995) 64

[21] Y. Tanaka, N. Ichimiya, Y. Onishi and Y. Yamada, Surf. Coat. Technol. 146-147 (2001) 215

[22] F. Vaz, L. Rebouta, P. Goudeau, J. Pacaud, H. Garem, J. P. Riviere, A Cavaleiro and E.Alves, Suf. Coat. Technol. 133-134 (2000) 307

[23] X. Hu, Z. Han, G. Li and M. Gu, J. Vac. Sci. Technol. A 20 (2002) 1921

[24] M. Konuma , H. Curtins, F.-A. Sarott and S. Veprek, Phil. Mag. B 55 (1987) 377

[25] R .A .Street, Phys. Rev. B 43 (1991) 2454

[26] W. J. Meng, X. D. Zhang, B. Shi, R. C. Tittsworth, L. E. Rehn and P. M. Baldo, J. Mater.Res. 17 (2002) 2628

[27] S. Veprek, A. Niederhofer, K. Moto, P. Nesladek, H. Männling and T. Bolom, Mater. Res. Soc. Symp. Proc. 581 (2000) 321

[28] J. Musil, H. Zeman, F. Kunc and J. Vlcek, Mater. Sci. Eng. A 340 (2003) 281

[29] Veprek S., in: Riedel R., ed, "Handbook of Ceramic Hard Materials", Wiley-VCH, Weinheim , p. 104-139 (2000)

[30] Banerjee R, Chandra R and Ayyub P 2002 *Thin Solid Films* 405 64

[31] Cullity B D 1978 *Elements of X-Ray Diffraction* (Reading,MA: Addison-Wesley)

[32] S. Veprek, Surf. Coat. Technol. 97 (1997) 15

[33] L. Hultman, J.E. Sundgren, J.E. Greene, J. Appl. Phys. 66 (1989) 536